PHOTOCATALYTIC DEGRADTION OF AZO AND RHODAMINE DYES USING NANOSTRUCTURED COPPER (II) OXIDE

ETCHU ESTHER MBU

(10601016)

DEPARTMENT OF MATERIALS SCIENCE AND ENGINEERING,

UNIVERSITY OF GHANA, LEGON

THESIS SUBMITTED TO THE DEPARTMENT OF MATERIALS SCIENCE AND ENGINEERING OF THE SCHOOL OF ENGINEERING SCIENCES, UNIVERSITY OF GHANA, IN PARTIAL FULFILMENT OF THE REQUIREMENTS FOR THE AWARD OF A MASTER OF PHILOSOPHY DEGREE IN MATERIALS SCIENCE AND ENGINEERING

2018

PHOTOCATALYTIC DEGRADTION OF AZO AND RHODAMINE DYES USING NANOSTRUCTURED COPPER (II) OXIDE

ETCHU ESTHER MBU

(10601016)

DEPARTMENT OF MATERIALS SCIENCE AND ENGINEERING,

UNIVERSITY OF GHANA, LEGON

THESIS SUBMITTED TO THE DEPARTMENT OF MATERIALS SCIENCE AND ENGINEERING OF THE SCHOOL OF ENGINEERING SCIENCES, UNIVERSITY OF GHANA, IN PARTIAL FULFILMENT OF THE REQUIREMENTS FOR THE AWARD OF A MASTER OF PHILOSOPHY DEGREE IN MATERIALS SCIENCE AND ENGINEERING

JULY 2018

Email: esthermichaiah@gmail.com

Supervisor

Dodoo Arhin David (PhD)

Senior Lecturer in Materials Science and Engineering

Department of Materials Science and Engineering

School of Engineering Science

University of Ghana

Accra – Ghana.

Co-Supervisor

Prof. Seteno Karabo O. Ntwampe (EngD, HDHET)

Associate Professor in Biotechnology and Head of Bioresource Engineering Research Group (*BioERG*)

Department of Biotechnology

Faculty of Applied Sciences

Cape Peninsula University of Technology

Cape Town – South Africa.

DECLARATION

I, Etchu E. Mbu, hereby declare that the contents of this thesis in its totality and originality is the result of research carried out by myself and supervised strictly by my main and co-supervisors in line with the University of Ghana's academic regulations and that no part of this work has previously been submitted to any institution for academic examination towards the award of any qualification.

Candidate	Date
Supervisor	Date
Co- Supervisor	Date
Head of Department	Date

ABSTRACT

Organic dye pollutants are sometimes released into the environment with wastewater from industries which make use of such dyes. In surface water, they contaminate the surrounding environment while their residue accumulates on land. These chemicals are noted for their toxicity to living organisms and they can cause cancers in human beings. In this study a relatively simple, long term and cost effective remedy for dye pollution reduction was developed; with a focus on the use of semiconductor photocatalysis for the breakdown of the dye in water. Due to their ease of synthesis, minimal toxicity and cost, copper (II) oxide (CuO) nanoparticles were used to degrade three commonly used dyes; Methyl Orange (MeO), Methylene Blue (MB) and Rhodamine B (RhB) which arise from two prominent dye families (Azo and Rhodamine dyes).

CuO nanoparticles were synthesised following a simple solution method using two copper precursor salts; hydrated copper sulphate ($CuSO_4.5H_2O$) and hydrated copper nitrate ($Cu(NO_3)_2.3H_2O$). The CuO was precipitated from a 0.02 M copper salt solution using 1.6 g/L NaOH pellets. The temperature at which these pellets were added to the copper salt solutions (25 °C and 60 °C) played a major role in determining the shape and size of the nanoparticles. The synthesised particles were then characterised using X-Ray Diffraction (XRD), Scanning Electron Microscopy (SEM), UV-Vis Spectrophotometry, Fourier Transform Infra-Red (FTIR) spectroscopy and Brunauer Emmett Teller (BET) surface area and porosity analysis. The synthesised nanoparticles were microporous with sizes ranging from 12 – 13.5 nm and BET surface areas of 26.8 m^2/g, 28.4 m^2/g and 49.3 m^2/g. The photocatalytic character of the synthesised particles was assessed in the presence of visible light for 100 minutes at 25-minute intervals and the overall minimum and maximum degradation efficiency recorded amongst all the samples was 85 % and 99 %.

Keywords: Nanoparticles; Copper Oxide; Photocatalysis; Wastewater; Dye; Degradation

ACKNOWLEDGEMENTS

My utmost thanks goes to the LORD God Almighty for giving me this life to live, for with it He gives all such good things as this Master's thesis. He never leaves me, even for a moment.

My appreciation also goes to the following people for their immense contribution towards the completion and success of this work:

- My supervisors Dr. Dodoo Arhin David for his dedicated supervision, transfer of skill and knowledge and Prof. Seteno Karabo O. Ntwampe for his dedicated supervision, transfer of knowledge and much needed "metal to the pedal" push.
- Dr. Agyeituffor Benjamin, Dr. Nyankson Emmanuel and Dr. Damoah Lucas of the Department of Materials Science and Engineering (DMSE) for their valuable input.
- The laboratory staff of the Department of Biotechnology of the University of Ghana for their ever- ready- to- help attitude throughout the time I worked in their lab.
- Mrs. Grace K. Akorful, the rest of the laboratory staff and laboratory National Service personnel at the DMSE for always assisting me.
- My loving and supportive family and friends. Thank you all for playing your God – assigned roles in my life on a daily basis.
- My sweet mother - Mrs Margaret E. N. Mbu whose unconditional love, ceaseless and fervent prayers have supported me through the years and still counting. My brothers - Rylance and Julius; your deep love, warm counsel and heartfelt prayers have not been in vain. My sister – Miranda, my other mother; your love and inestimable sacrifices over the years have catapulted me into this achievement.
- Béni Lutonadio - my love, my husband, my partner in prayer and purpose; Thank you for believing in all that God has put in me. We made it!

Esther E. (Mbu)Lutonadio

DEDICATION

To my loving husband – Béni

And

To the blessed memory of our departed heroes who gave us the best of their lives here on earth and who then went to be with the Lord; our beloved parents:

Colette Kiabanguka Lufunda and **Bernard Oben Mbu**

Forever in our most treasured memories.

TABLE OF CONTENTS

TABLE OF FIGURES

LIST OF TABLES

GLOSSARY

Abbreviations	Definition
AAs	Aromatic Amines
TMOs	Transition Metal Oxides
RT	Room Temperature
MeO	Methyl Orange
MB	Methylene Blue
RhB	Rhodamine B
IUPAC	International Union of Pure and Applied Chemistry
CB	Covalent Band
VB	Valence Band
BET	Brunauer–Emmett–Teller
FTIR	Fourier Transform Infra-Red
SEM	Scanning Electron Microscopy
XRD	X-Ray Diffraction
TGA	Thermogravimetric Analysis
UV	Ultra Violet Light
Vis	Visible Light

CHAPTER ONE

1.0 Introduction

1.1 Background to the study

With the fast - growing world of technology today, man's needs have become more numerous with specific needs for dyed products thereby placing high levels of stress on the environment due to pollution. Amidst all these anthropogenic activities, the release of undesired pollutants and waste into the environment is inevitable. Unwanted end or by-products of any production process usually end up in the wastewater released by the producer. Waste is therefore an integral part of any production process and can be either non-toxic or toxic to man and/or his environment. There is certainly little or no cause for alarm when non-toxic waste is produced. Contrarily, any waste that is potentially toxic is of great concern and if there is no feasible way to carefully treat and/or reduce the toxicity of waste generated during the production process, then an alternative method of production (without compromising the value of the product) must be found to adequately treat and dispose of the waste produced at the end of the production chain. This will be mainly to reduce any form of pollution.

Pollutants and the extent of their toxicity will vary from one industry to another depending on numerous factors, some of which include; the raw materials, processes involved in production and the desired final product. Among some raw materials, dyes are essential to the aesthetic appeal of the final product and are widely used by numerous industries (textile, food, automobile and pharmaceutical industries) today. They can be broadly classified into acidic, basic, direct, fluorescent, disperse and metal complexed dyes among others[1],[2] or simply as Natural or Synthetic dyes when their classification is based on their origin/source. Dyes are

used across a wide number of industries (Food, cosmetics, leather, paper, pharmaceutical and textile amongst others) with the textile industries being the biggest dye consumer amongst all these industries[1], [3].

Today, there exists over 3000 known types of commercially available dyes and half of these dyes are classified as "Azo dyes"[4], [2]. These are the most used in the textile industry making up 60 – 70 % of the global dye population used[5],[3]. Like most other synthetic dyes, Azo dyes are toxic to humans especially if not properly degraded in wastewater prior to disposal. The resulting partially degraded by-products be even more toxic to man than the parent compound[2]. Examples of some Azo dyes include Methyl Orange (MeO), Methylene Blue (MB) and Trypan blue[6],[7].

Similarly, another well-known class of widely used dyes are the Rhodamines. They are commonly used in the textile, leather, paint and even printing industries. Examples of such dyes include Rhodamine 6G, Rhodamine 123 and Rhodamine B (RhB). RhB like most dyes is commonly used in printing and staining fluorescent probes in research laboratory applications[8],[9].

To effectively meet the (often huge) potable water requirements associated with dye-related processes, most of the industries make use of facilities near water bodies such as lakes, rivers and wells where there is a ready supply of the primary raw material i.e water[5], [10]. This proximity or nearness-to-water supply bodies puts these water bodies at risk of contamination from improperly treated waste and/or wastewater. This could also happen to the surrounding soils into which such water may progressively seep over time[11]. This has proven to have far reaching consequences such as harming aquatic organisms whose habitat is ecologically reliant on these water bodies making bioaccumulation prevalent as some of these animals are edible to man[2], [12].

To mitigate against such pollution, photocatalytic degradation on suitable matrices is advised. Amongst other techniques employed in wastewater treatment in recent years is heterogeneous photocatalysis. It is a method which makes use of nanomaterials and is proven to be very effective in the degradation of wastewater organic pollutants such as azo dyes[13]. Semiconductor materials have been found to be particularly effective as catalysts in these photon-facilitated reactions. This is because they are able to both adsorb the pollutant and absorb photons of light, forming free radical species in solution which facilitate the degradation of the undesired pollutants into carbon dioxide (CO_2), water (H_2O) and non-toxic inorganic ions[14].

Several methods have been employed for the synthesis of these semiconductor nanomaterials. In this era, after considering the possible efficiency of desired semiconductor nanomaterial, the cost (from synthesis to application) is an important factor to consider because one of the primary objectives is also to be able to commercialise an affordable (cutting across all social classes) product to the consumers. In recent times, some of the simplest (cheap), yet effective methods are chemical solution methods for the synthesis of nano-semiconductors and this study examined one such method applied in a study by Zhu et al.[15].

In recent years, South Africa (2017-2018) and Ghana are two countries in Africa which have faced alarming threats of water crisis necessitating the recycling of wastewater. The latter at the time of this research still faced a looming threat of the lack of freshwater source availability in the near future[16],[17],[18]. These are specific cases but on a global scale, the United Nations has put forward a suggestion that forty-one countries were victims of water stress in the year 2011 and some of these are nearly facing exhaustion of their renewable freshwater supplies[19]. Overall, 40% of the global population is affected by water scarcity and the said suggestion also projected a rise in this percentage in the near future due to climate change. More so, an estimated 80% of wastewater produced from human activity is deposited into

rivers, seas or other water bodies without adequate treatment due to limited monitoring [20]. The consequences of such actions cannot be overemphasised as they have become glaring making the need for adequate wastewater treatment and/or disposal techniques a necessity. Immediate action for water preservation needs to be taken to protect our water-related ecosystems. As such, we need to develop readily adaptable technologies for use even in remote areas show proof of individual responsibility too. This research is therefore inspired by the desire to contribute towards the development of more adequate, environmentally benign and cost efficient techniques for wastewater treatment, hence to protect our environment and conserve our water resources.

1.2 Research Problem

Azo and rhodamine dyes are some of the most widely used dyes in the textile, paint and printing industries with the azo dyes alone making up 60 - 70 % of the total dye population used[5],[3],[8],[9]. Like most other synthetic dyes, these two classes of dyes are toxic to humans especially if not properly degraded in wastewater prior to disposal. Sometimes the resultant by-products of partial degradation of these dyes can be more toxic to man than the parent compound[2].

However, because of the huge need for potable water required during the production processes in these dye-consuming industries, their facilities are often situated close to water bodies to allow for easy access. Such water bodies end up being contaminated by the release of improperly treated wastewater containing such dyes or the products of their incomplete breakdown into these waters[5],[10]. Such contamination has resulted in great harm to aquatic organisms which rely on these water bodies for their livelihood[12]. There is therefore the need

for adequate technologies for the complete degradation of these dyes into non-toxic end products.

1.3 Hypothesis

Azo and rhodamine dyes can efficiently be degraded photocatalytically by using CuO nanoparticles synthesised by a simple chemical method without the use of surfactant.

1.4 Aims and Objectives

This research was geared towards finding a permanent solution to the concerns arising from the release of certain organic dyes into the environment through wastewater from industries. It involved the use of nano-semiconductor facilitated photocatalytic degradation of these organic pollutants in water to limit their release into the environment. The research exploited the photocatalytic degrading strengths of the CuO nanoparticles synthesised under three different conditions using a simple solution chemistry technique. There was a focus on the degradation of MeO, MB and RhB dyes; thereby, assessing any differences in the degrading efficiency of each batch of the synthesised nanoparticles in the process. In summary, the aims and objectives include:

Aim 1: Synthesis and characterisation of CuO nanoparticles.

Objective 1: Synthesise CuO nanoparticles using a simple solution chemistry technique without the use of surfactant.

Objective 2: Study the properties and characteristics of the synthesised CuO nanoparticles.

Aim 2: Photocatalytic application of the synthesised CuO nanoparticles.

Objective 1: Study the efficiency of each CuO nanoparticle sample in the degradation of the selected dyes (Methyl Orange, Methylene Blue and Rhodamine B).

1.5 Significance of the study

This research investigated the efficiency of CuO nanoparticles synthesised from a simple chemical method in the degradation of selected organic dyes in water. The study therefore puts forth a technique to facilitate the elimination of such organic dyes from industrial and household wastewater.

1.6 Delineation of the study

The aspects below were not covered in detail during this study.

- The detailed application of the study in industrial process workflow.
- The effect of the synthesised CuO nanoparticles on organic pollutants which do not belong to the classes of the selected dyes.
- The effect of the temperature and pH of the water on the degradation process.

CHAPTER TWO

2.0 Literature Review

2.1 Photocatalysis

Every potential chemical reaction requires a minimum amount of energy in order for it to occur. This minimum energy required for a reaction to occur is called the Activation Energy and is particular to the given reaction under well-defined conditions. This energy can be supplied through a number of ways (including as photons) depending on the reaction system. Photocatalysis is a phenomenon whereby, an illumination source supplies energy in the form of photons (hence, the prefix "photo"), which serves to activate a catalyst in a catalysis reaction (reaction involving a catalyst); hence, the suffix "catalysis". By IUPAC definition, a catalyst is any substance which can enhance the rate of a chemical reaction without taking part in the reaction itself. Therefore, it is neither altered nor consumed during the reaction. In a photocatalytic reaction, the catalyst is particularly called a photocatalyst. An example of a naturally occurring photocatalytic reaction is photosynthesis, whereby, the catalyst is chlorophyll which absorbs and uses photons from the sun for the production of food for the plant[21]. Another non-natural but equally spontaneous example of this phenomenon is the deterioration of titanium dioxide (TiO_2)-containing paint films on buildings by photocatalytic activation of the TiO_2 after absorbing solar energy over time, leading to the degradation of the paint with time[22].

Soon after some of these naturally occurring and accidental (unplanned) photocatalytic reactions were observed, scientists researched them, focusing on their efficiency and their potential applications. The phenomenon became attractive as it proved to be useable since:

- It has low energy requirements compared to those of conventional methods (such as thermal degradation for example) which have high energy requirements. This method can therefore be described as energetically sustainable[22].
- It can be used in all three phases, i.e solid, liquid and gaseous phases of matter, offering pollutant treatment at source; thereby, degrading them (pollutants) partially or completely into harmless / less harmful substances and minimising secondary waste/pollutant production while offering the possibility of recovery and even reuse (recycling) of the photocatalyst[22].
- One of the target sources of energy in most cases of photocatalysis is clean solar energy making this method cost efficient and relatively eco-compatible (environmentally benign)[23].

Nowadays, one of the most exploited and yet still promising areas of photocatalysis application is in the treatment of wastewater, an area whereby semiconductor photocatalysts have been widely used[24]. For such a physico-chemical process to succeed, the basic underlying process would involve the promotion of an electron from the valence band (VB) to the conduction band (CB) of the chosen semiconductor using a photon (packet of energy) from an illumination source[25]. For this electron promotion to occur, the energy supplied should be equivalent to or greater than the energy of the "bandgap" (energy gap between the VB and CB) of the semiconductor. This energy is the minimum activation energy required for an electron to be dislodged and is semiconductor dependent; with the loss of an electron from the VB resulting in an aperture and the creation of an electron-hole pair (see Figure 2.1).

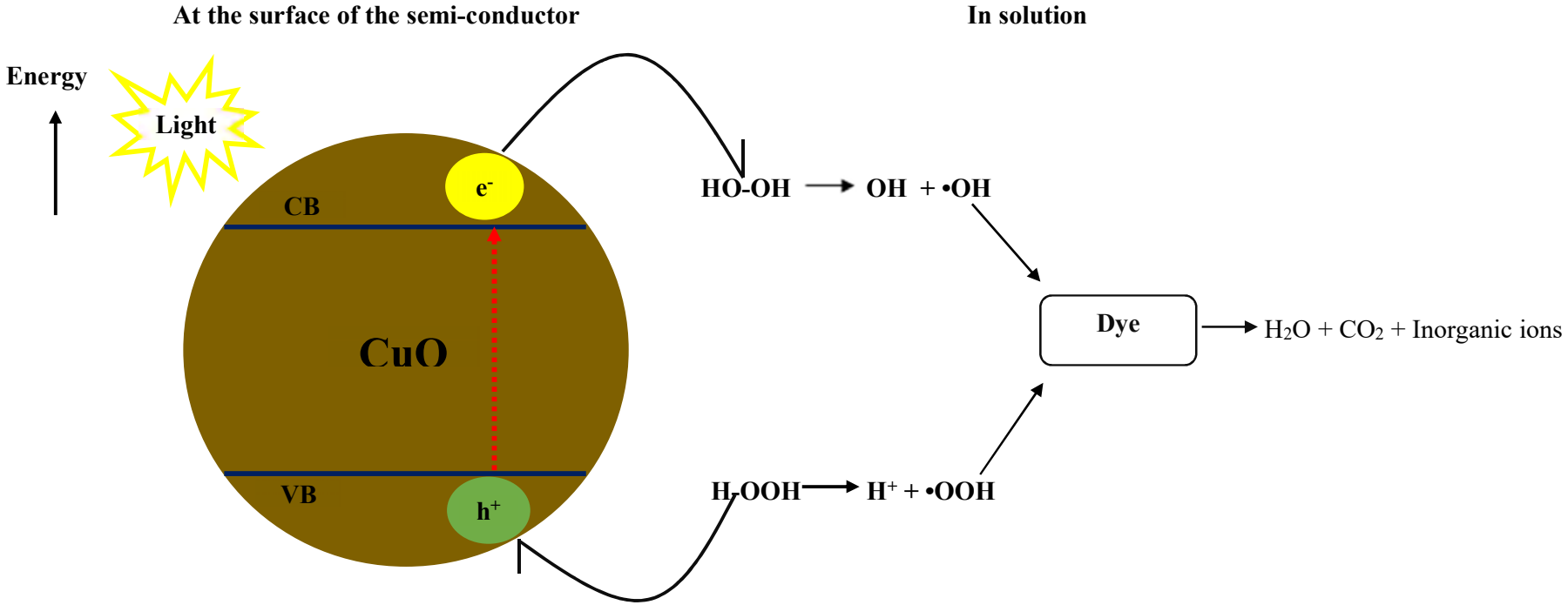

Figure 2.1: Simple representation of an electron-hole pair formation in CuO and the resultant free radical formation and consumption in the dye break-down process in solution, in the presence of H_2O_2

(CB and VB stand for Covalent Band and Valence Band respectively)

Examples of some of the semiconductors which are frequently used in photocatalysis include TiO_2[1], [23], [25], Cu_2O[26], [27], SnO[6],[28], ZnO[26] with some like CuO gaining popularity in recent times[15], [29]–[32]. It has been found that CuO is suited for use in the presence of hydrogen peroxide (H_2O_2) [33] which enhances degradation by readily splitting into free radicals when attacked by electrons and/or holes.

A proposed mechanism for photocatalysis using CuO as a photocatalyst is shown in Figure 2.1 whereby the electron and subsequent aperture (hole) formed interact with the H_2O_2 resulting in the formation of free radicals which in turn oxidise the pollutant forming intermediates that can be mineralised to carbon dioxide, water and inorganic ions. In research as in other semi-conductor catalysed processes, the process is said to be a heterogeneous photocatalysis reaction because the catalyst (semi-conductor) and pollutant are in two different phases during the reaction, i.e solid and liquid, respectively[34].

2.2 Copper oxide (CuO): Structure and its potential as a photocatalyst

CuO, otherwise known as *cupric oxide* is a p-type transition metal oxide semiconductor which represents one of the two stable forms of the oxides of copper (CuO and Cu_2O). Its chemical formula CuO, immediately highlights the fact that in this molecule, copper has a +2 oxidation state; hence, the systematic name *copper (II) oxide*. Despite the numerous differences in their physical and chemical properties (bandgap, unit cell structure, conductivity and space group), they are similar to each other in that they both have applications in almost the same areas, some of which include: gas sensors, photovoltaics, catalytic oxidation of CO and other heterogeneous catalysis. This is because though different in chemical composition, they are alike as they are nontoxic, have a low forbidden gap energy and a low synthesis cost with good catalytic and optical absorption properties. However, CuO has an added advantage in that it has a relatively stable structure at ambient temperature when compared to the Cu_2O[33].

In 1933, the CuO crystal structure was originally illustrated by Tennel and later in 1970 single-crystal techniques were used to elucidate intricacies associated with the structure of this compound[33]. Described as *tenorite,* it has a monoclinic crystal structure, in which the atoms within each crystal have a coordination number of four arising from the fact that each Cu atom is surrounded by four oxygen atoms [35].

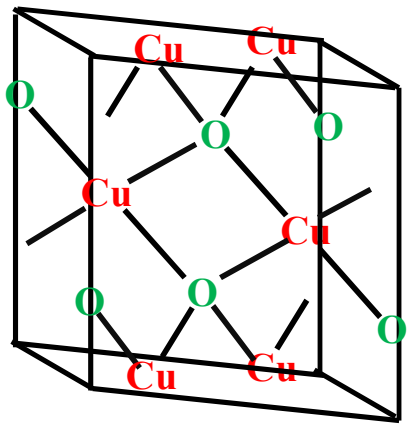

Figure 2.2: Monoclinic structure of CuO adapted from[33]

Its energy bandgap has experimentally been found to range between 1.2 eV to 1.7 eV (bulk material) with the possibility of an increase in the band gap with a decrease in the size of the individual particles, particularly at nanoscale; a phenomenon known as "Quantum Size Effect"[33], [36], [37]; a phenomenon whereby the crystal's size is inversely proportional to the bandgap energy. There generally exists inter-atomic interactions in the bulk CuO material but these decrease as the size of the particles decrease. This trend can be accounted for by the behaviour of the energy levels of nano scale particles as those of isolated atoms owing to how small they become at the nano level compared to the size of crystallite in the bulk material. These form a continuous spectrum of discrete energy levels, which are farther apart from each

other than they would be in the bulk material. When agglomerated, these discrete energy levels result in a widening of the energy gap of the nanomaterial compared to that of the bulk material; a quantum size/confinement effect[35][36].

Compared to other Transition Metal Oxide (TMO) nanomaterials, CuO has a greater number of applications in heterogeneous catalytic conversions of hydrocarbons into carbon dioxide, amelioration of the ability of nanofluids to conduct heat, nanomaterials for energy applications and in the formation of super-hydrophobic surfaces with particularly intriguing properties in the domains of magnetism and super-hydrophobicity[33], [38]. As photocatalysts, CuO nanomaterials have been found to exhibit high surface areas, high porosity and recyclability[39] which makes them good degraders of organic pollutants.

2.3 Synthesis and photocatalytic applications of CuO nanoproducts

Over the years, numerous technics have been used to synthesise CuO nanostructured materials of variable morphologies with significant and differentiated photocatalytic ability either with or without the use of surfactants and/or templates. Some early techniques include rapid precipitation, hydrothermal, solvothermal, sol-gel, sonochemical while recent techniques make use of methods such as microwave irradiation to synthesise these nanoproducts mostly because of the rapidity and relatively low energy requirements of such procedures[13], [28], [40]–[43].

For instance, a precipitation method can be used without surfactant supplementation or templates to produce dandelion-like nanoparticles with a narrow particle size distribution of 20-30 nm diameters and a 1.65 eV band gap, which can degrade (in UV and visible light) a 5 mg/L Methylene Blue solution to about 0.14 mg/L, a 97.3 % photocatalytic degradation efficiency within 3 hours[44]. Another study revealed a 96.7 % degradation efficiency on RhB dye after 9 hours in UV light when some sheet-like CuO nanoparticles, with 15 nm diameters

and a 2.31 eV bandgap were prepared at ambient temperature using a simple solution method[45]. In another study, it was found that CuO nanowires of diameters less than 50 nm and a 1.85 eV band gap were used to degrade a 20 mg/L Methyl Orange solution resulting in a 90 % degradation within 3 hours using natural light[46].

Amongst others, wet chemical methods stand-out because of their relatively low-cost, non-toxicity and a high yield which minimises wastage of the raw materials while accurately controlling the shapes and sizes of the nanoproducts synthesised[47][15]. It has been found that the latter, which defines the morphology of nanomaterials in combination with other factors such as the how much of the high energy surface is exposed for reaction, would determine the photocatalytic activity, thus the efficiency of the nanomaterials in general[48], and for CuO in particular[33]. Zhu et al.[15] recommended a simple cost efficient solution method which unites all the factors listed above and which could yield photocatalytically efficient CuO nanomaterials. The procedure was used for the synthesis of the nanomaterials and the recommendation for photocatalytic application was carried out in this research.

2.3.1 Solution method without surfactant

To minimise cost, controlling the morphology of the end product and still maintaining a reasonable yield, this research is fundamentally based on a simple solution method which excludes the use of surfactants as described by Zhu et al. [15]. The original procedure involved the use of a $Cu(NO_3)_2.3H_2O$ solution to which NaOH was added at different temperatures (2, 25, 60 and 100 °C), to precipitate CuO nanomaterials. They concluded that the supplementation of NaOH at varying temperatures is and influential synthesis parameter which effectively determines the final shape/morphology of the synthesised nanomaterials.

This research followed the fundamental synthesis procedure presented by Zhu et al.[15]; albeit with numerous novel modifications being implemented which are:

- Unlike the original procedure which used only $Cu(NO_3)_2.3H_2O$, this research used two precursor salts ($Cu(NO_3)_2.3H_2O$ and $CuSO_4.5H_2O$), as changing the precursor copper salt ($Cu(NO_3)_2$ and $CuCl_2$), led to a change in morphology and chemo-physical properties of the synthesised CuO nanomaterials in one such study[49]. Therefore the strategy of this synthesis was implemented to primarily investigate whether there would be any differentiation in morphology and in application efficiency of the resulting CuO nanomaterials from the precursor salts used.
- This research further to determined how effective the obtained CuO nanomaterials are in the degradation of a number of organic dyes from two different functional groups, i.e azo and rhodamines which are recalcitrant water pollutants[50].

The synthesis was determined to not be adversely affected by the absence of a surfactant based on a study conducted by Tran et al.[28], that though surfactants would minimise agglomeration of the synthesised nanoparticles, simply varying the concentration of the reactants could play the same role resulting in controlled size, morphology consistency and ease of separation between the synthesised nanostructures. This method therefore minimised cost while achieving the desired size, variety and quality by lowering the precursor salt concentrations to ensure a uniformly spread particle size distribution range. The reason for an inexpensive thesis today is that this research is developed for further use in large scale purification and/or pollutant degradation systems in numerous industries including for household purification or for use in remote areas with decentralised water systems.

A general direct-solution-method route for the synthesis of CuO nanostructured materials can be described by the Equations 2.1 and 2.2[28].

Copper salt + Alkaline hydroxide → $Cu(OH)_2$ + Salt of alkaline metal 2.1

$Cu(OH)_2$ → CuO + H_2O + inorganic ions in solution 2.2

2.4 Dyes

Whether of synthetic or natural origin, dyes have one common characteristic which man exploits; colouring for aesthetics of final products. According to certain studies, it has been found that at least 10 – 15 % of the total amount of dye used during the dying process is lost in one way or another during the dyeing process. Most of these are released into the aquatic environment resulting in bioaccumulation in living organisms with biomagnification ensuing through the food chain. Despite the numerous stringent measures that have been put in place both by international bodies and individual nations to limit this environmental health challenge, some of these dyes seem almost indispensable to their users. Azo dyes are a typical example of a highly toxic, widely used class of organic dyes[2]. In this study, the degradation of three different dyes (MeO, MB, RhB) in solution using the synthesised CuO nanoparticles was studied with the aim for application in wastewater treatment; systems which contain large quantities of recalcitrant dyes.

2.4.1 Methyl Orange (MeO)

MeO is of the family of azo dyes. They are synthetic [2] and contain the characteristic azo (-N=N-) group. The single bonds indicated on the nitrogen atoms can be links to an alkyl (R) or aryl (R') functional group as shown in Figure 2.3. They are used in many industries today ranging from food, pharmaceuticals, petroleum products and textiles. Albeit, the textile

industry is reportedly the leading consumer of dyestuff, 60-70% of their consumption being made up of azo dyes [4], [5], [51].

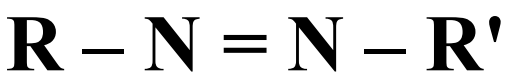

Figure 2.3: General chemical structure of an azo compound

Azo dyes are often preferred due to their ease of synthesis, with ready adherence to different materials being dyed, with long lasting and permanent aesthetics once applied to products as opposed to their natural counterparts. They generally offer a greater variety of colours[2]. These dyes have also been found to be toxic both to man and to the environment when discarded or released in liquefied matrices. Their incomplete breakdown could result in any one of about thirty six possible aromatic amines (AAs) which are classified in public databases as toxicants. For instance, AAs which have mutagenic or carcinogenic properties in the human body can be released when these compounds are degraded by various skin bacteria[5], [1].

Methyl Orange (Figure 2.4) is an azo dye with multi-industrial applications. Otherwise known as sodium;4-[[4-(dimethylamino)phenyl]diazenyl]benzenesulfonate (IUPAC), orange III or gold orange, this compound is not only used in textiles as a dye, but also in chemical laboratories as a pH indicator in acid-base titrations[52].

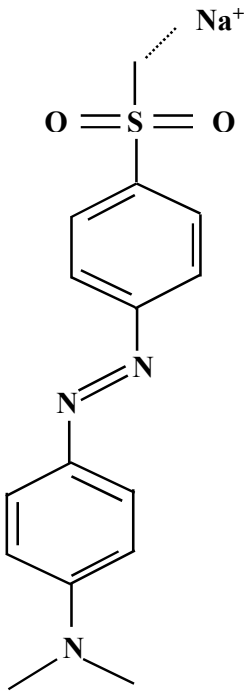

Figure 2.4: Chemical structure of Methyl Orange adapted from [52]

Research has been done towards safe and complete degradation of this dye mostly using TiO_2 alone[53], TiO_2 doped with other metal catalysts[54]–[56], TiO_2 associated with carbon nanotubes[57]; ZnO both alone[58] and doped [59]; iron (Fe) alone[60] or in Fenton reactions[61], [62] and with naturally occurring biological species such as *Eichhornia crassipes*[63] and *Kocuria rosea*[64], to name a few. Generally, a lot of research has already been done and is still being conducted with these semiconductor catalysts sometimes in combination with biological degraders, with the main challenge being that the dye sometimes is a metabolic inhibitor to the potential degraders, given that they are living organisms[53].

Minimal has been done using CuO as a photocatalyst when it comes to MeO degradation. Liu et al.[46] prepared CuO nanowires on a Cu-foil substrate which were able to reduce 20 mg/L MeO solution in natural light by 90 % after 3 hours. Sasikala et al.[6] degraded a MeO dye solution over 5 hours using cerium-loaded CuO nanoparticles in UV light. Similarly, Hua et al.[65] degraded a 2 g/L MeO dye solution by about 70 % within 2 hours using gamma- Al_2O_3 impregnated CuO. These studies all demonstrate the efficiency of using nanostructured CuO in the degradation of azo dyes.

2.4.2 Methylene Blue (MB)

Being a derivative of the azo family, MB is classified as an azo dye despite the fact that the –N=N- functional group is not present in its structural formula[66],[50]. It is used as a bacteriological dye [67],[68], as a drug in medicine and as an indicator[68]. Otherwise known as [7-(dimethylamino)phenothiazin-3-ylidene]-dimethylazanium;chloride (IUPAC) or Methylthioninium Chloride, it has the chemical formula $C_{16}H_{18}C_lN_3S$ with a chemical structure as shown in Figure 2.5[68].

Bubacz et al.[50] investigated the photocatalytic degradation of MB using anatase phase TiO_2, while Ameta et al.[69] used CaO. Similarly, Houas et al.[70] used TiO_2 in UV to degrade MB and another study indicated that the dye can also be degraded using CuO nanoparticles[71] and nanocrystalline TiO_2 loaded with CuO[72].

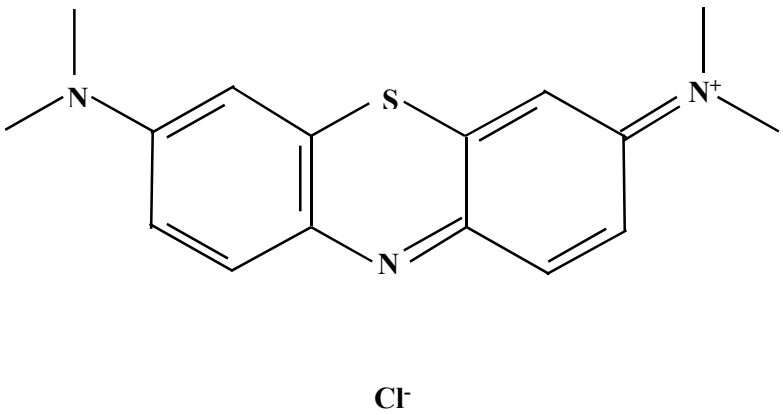

Figure 2.5: Chemical structure of Methylene Blue adapted from[68]

2.4.3 Rhodamine B (RhB)

Also known as Tetraethylrhodamine or [9-(2-carboxyphenyl)-6-(diethylamino)xanthen-3-ylidene]-diethylazanium;chloride (IUPAC), this compound is a synthetic dye with chemical formula $C_{28}H_{31}C_lN_2O_3$ (Figure 2.6). It belongs to the family of xanthenes[9] and its crystals can appear dark green or reddish violet (powder). It is used as a dye in the paper industry, in pharmaceuticals, cosmetics and as a chelating agent[73].

Petal and flower-like CuO nanostructures[74] as well as nanorods and nanowires[75], have all been applied in the catalytic degradation of RhB. Studies have also been carried out towards the photocatalytic degradation of RhB dye using CuO nanosheets[76] and nanoparticles[77]. It is necessary to ensure that the dye is completely broken-down into non-toxic end products[5]. There is therefore, a need to develop techniques appropriate not just for the safe decolouration but also for the complete degradation of these dyes without resulting in any toxic degradation end products[12].

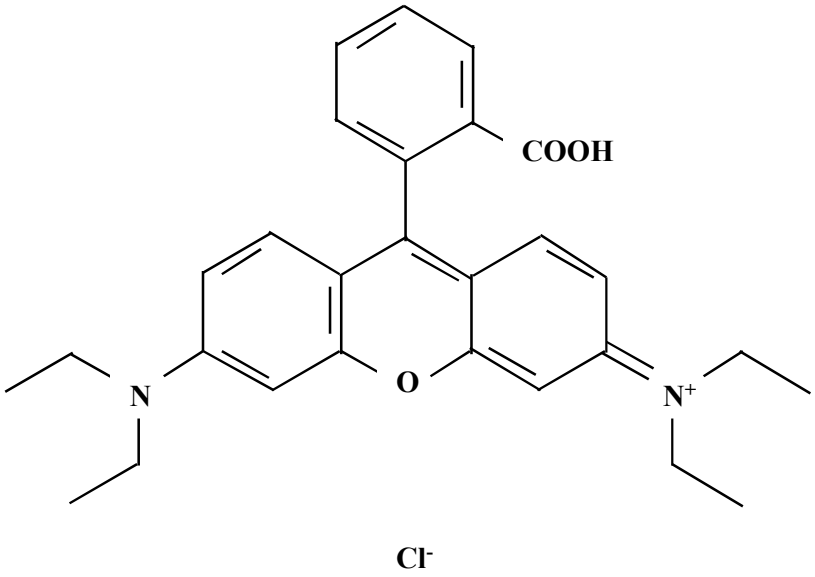

Figure 2.6: Chemical structure of RhB adapted from [73]

Until minimal toxicity is attained, it can be said that part of the relevance of this research study contributes towards the development of more effective techniques for the treatment of wastewater from industries which make use of the dyes discussed herein.

CHAPTER THREE

3.0 Materials and Methods

3.1 Reagents

Analytical grade reagents were used throughout this research study. They included hydrated copper nitrate ($Cu(NO_3)_2.3H_2O$) (Sigma-Aldrich Co., Germany), hydrated copper sulphate ($CuSO_4.5H_2O$) (Breckland Sc. Supplies, UK), sodium hydroxide (NaOH) (Qualikems Fine Cem Pvt Ltd, India), methyl orange (Fizmerk India Chemicals, India), methylene blue (KEM Light Laboratories Pvt Ltd, Mumbai-India), rhodamine B (Paskem Finechemicals Industry, India), 30 % hydrogen peroxide (Merck, Germany) and ethanol (Fisher Scientific, UK). The water used was deionised to reduced interference in the research undertaken.

3.2 Synthesis of CuO nanomaterial

As briefly introduced in Chapter 2, CuO was synthesised from three different reactions following a simple solution method and involving three distinct reagents; two different copper precursor salts (($Cu(NO_3)_2.3H_2O$) and ($CuSO_4.5H_2O$)) and NaOH. In each case, the ration of copper precursor salt to NaOH was 1:2 and all the copper precursor salts were dissolved in deionised water to prepare 0.02 M solutions to which 1.6g/L M NaOH was added to precipitate CuO via a copper hydroxide ($Cu(OH)_2$) intermediate. The overall reaction process can be further broken down into 3 basic, general, stoichiometric equations represented by 3.1, 3.2 and 3.3 below for the purpose of understanding the chemistry involved.

$$Cu_yX_2 . zH_2O_{(s)} + H_2O_{(l)} \longrightarrow Cu^{2+}{}_{(aq)} + 2X^{-y}{}_{(aq)} \qquad 3.1$$

$$Cu^{2+}_{(aq)} + 2NaOH_{(aq)} \longrightarrow Cu(OH)_{2(aq)} + 2Na^{+}_{(aq)} \qquad 3.2$$

$$Cu(OH)_{2(aq)} \xrightarrow{\Delta} CuO_{(s)} + H_2O_{(l)} \qquad 3.3$$

Where *X* is the corresponding anion in the copper precursor salt with a *–y* oxidation state and *z* represents the number of moles of water in the hydrated copper salt. Equations 3.4, 3.5 and 3.6 further summarise steps 1, 2 and 3 listed above for all three distinct reactions.

$$Cu(NO_3)_2.3H_2O_{(aq)} + 2NaOH_{(s)} \xrightarrow[\Delta]{60\ ^\circ C} CuO_{(s)} + 2NaNO_{3(aq)} + 4H_2O_{(l)} \qquad 3.4$$

$$CuSO_4.5H_2O_{(aq)} + 2NaOH_{(s)} \xrightarrow[\Delta]{60\ ^\circ C} CuO_{(s)} + Na_2SO_{4(aq)} + 6H_2O_{(l)} \qquad 3.5$$

$$CuSO_4.5H_2O_{(aq)} + 2NaOH_{(s)} \xrightarrow[\Delta]{25\ ^\circ C} CuO_{(s)} + Na_2SO_{4(aq)} + 6H_2O_{(l)} \qquad 3.6$$

In each case, the entire reaction proceeds under continuous stirring conditions. In the reactions represented by Equations 3.1 and 3.2, the 0.02 M aqueous solution of copper salts were heated till the solution got to a temperature of 60 °C after which NaOH pellets were added. The formation of a milky blue $Cu(OH)_2$ precipitate ensued rapidly and was observed to last only a few seconds as the solution quickly turned blue black due to the formation of CuO. Within a few minutes the entire solution which was initially blue had completely turned black. The solutions were maintained at precipitation temperature for another 10 minutes (after addition of the NaOH pellets) then they were heated further to 100 °C and again maintained at this temperature for 10 minutes to allow for the complete precipitation of CuO. After this, the product was allowed to cool then it was centrifuged and washed with a 1:1 water and a distilled

ethanol solution several times. The precipitate was finally washed with water and oven dried (70 °C) until a consistent weight was attained.

In the case of Equation 3.3, 1.6g/L NaOH pellets were added to the 0.02 M copper sulphate salt ($CuSO4.5H_2O$) solution at ambient temperature (typically 25 °C). The reaction was allowed to proceed at this temperature for 10 minutes after the addition of the NaOH pellets. During this time, the formation of a milky blue copper hydroxide ($Cu(OH)_2$) precipitate was observed with minimal black precipitate being formed. After these 10 minutes, the solution was heated to 100 °C and maintained at this temperature for another 10 minutes. During the time the solution was being heated to 100 °C, the milky blue solution was observed to progressively turn black as a CuO precipitate was formed. Analogous to the previous procedure, the black solution was subsequently centrifuged and rinsed with water and a distilled ethanol (1:1) solution several times then finally rinsed with water and oven dried (70 °C) to obtain CuO powder. Figure 3.2 summarises the procedure for the synthesis of the CuO nanoparticles while Figure 3.3 (a), (b), (c) and (d), (e), (f) represent the pre- and post- synthesis of the CuO nanoparticles prior to washing and drying.

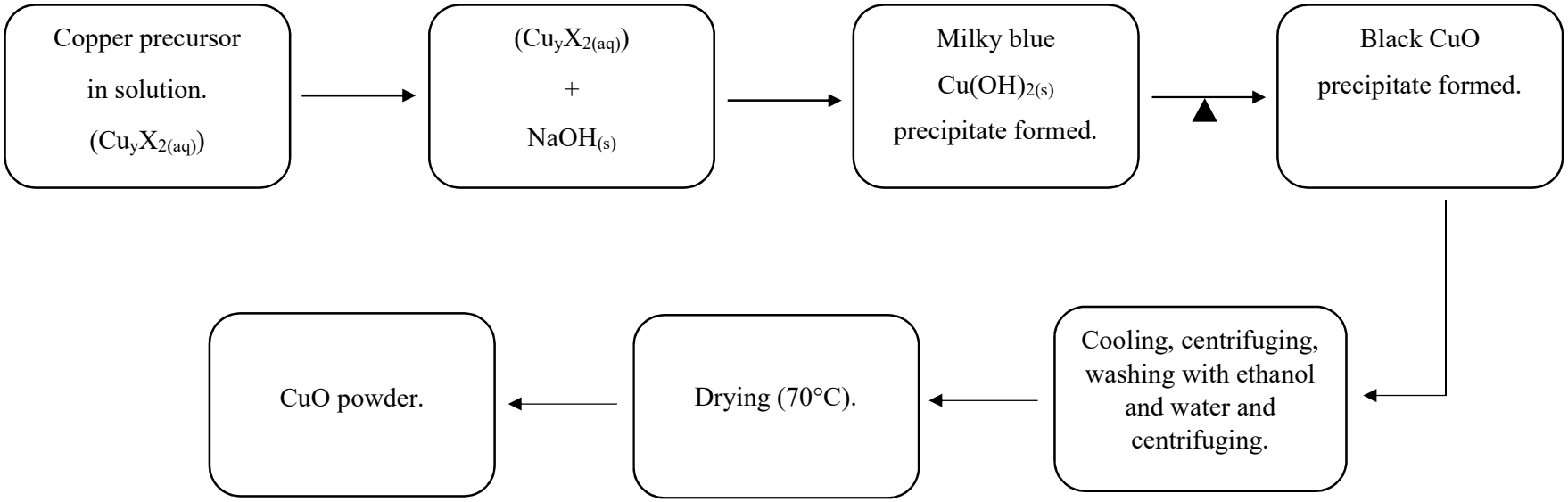

Figure 3.1 Simplified workflow diagram for synthesis of nanostructured CuO

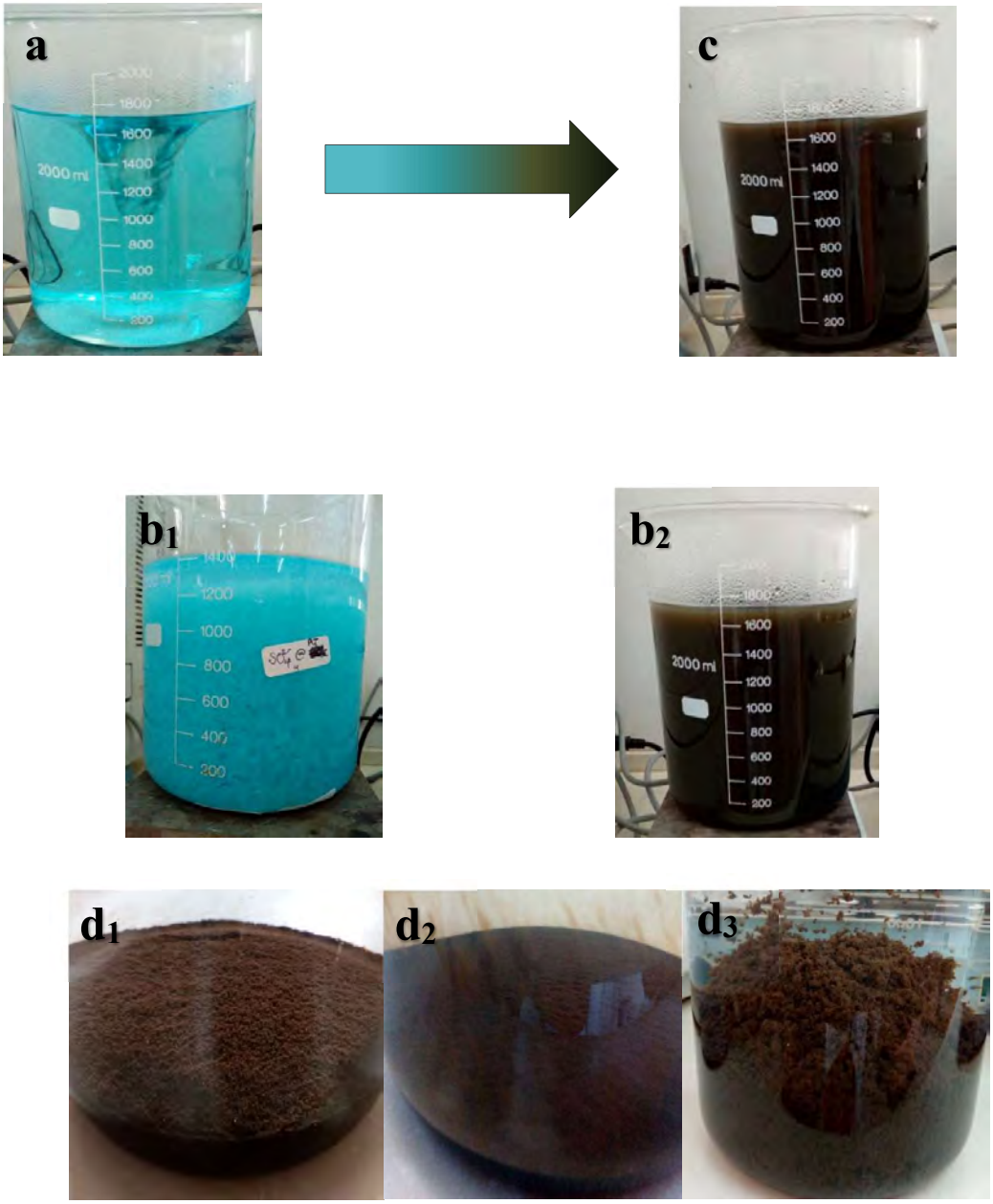

Figure 3.2: CuO synthesis process. (a) Initial copper salt solutions before addition of NaOH, (b_1) Formation of $Cu(OH)_2$ intermediate after addition of NaOH at 25 °C, (b_2) Formation of CuO after addition of NaOH at 60 °C, (c) Final copper salt solutions after addition of NaOH and heating to 100 °C, (d_1) CuO from $CuSO_4.5H_2O$ at 60 °C NaOH adding temperature (d_2) CuO from $Cu(NO_3)_2.3H_2O$ at 60 °C NaOH adding temperature (d_3) CuO from $CuSO_4.5H_2O$ when NaOH is added at 25 °C

3.3 Analytical instruments for characterisation

Amongst the techniques used to determine the properties of the synthesised CuO nanomaterials, crystallite size and crystal growth planes were determined using X-Ray Diffraction (XRD) studies using an X'Pert PRO X-Ray Diffractometer (PanAnalytical, the Netherlands) operating with Cu K-α radiation (wavelength of 1.544 Å) at 45 kV and 40 mA with a 20 - 70° 2θ range, a 0.2° step width scanning 1.2 deg/min on a 2 g sample. Absorbance was measured using a UV-Vis spectrophotometer (Thermo Fisher Scientific, China) operating within a scanning range of 200 – 900 nm with a 5 nm scan step on a 3 ml sample. Surface morphology of the samples were studied using a Scanning Electron Microscope (SEM) – TESCAN with EDX analysis software (Performance in Nanospace, Czech Republic) operating at within 0.2 – 30 kV and $2x10^{-5}$ ms – 10 ms per pixel scanning speed on a 0.5 g sample. Fourier Transform Infra-Red Spectroscopy was performed using a PerkinElmer Spectrum Two spectrometer (PerkinElmer Inc., UK) with a 4000 – 400 cm^{-1} scanning range and 4 cm^{-1} resolution on a 0.1g sample. Brunauer–Emmett–Teller (BET) surface area and porosity analysis were carried out using (i) An ASAP 2020 V4.01 for CO_2 adsorptive analysis (Micrometrics, USA) and (ii) A Tristan II 3020 version 2 (Micrometrics, USA) for N_2 adsorptive analysis, on 0.4 g samples.

3.4 Photocatalytic Degradation

A dye solution (10 mg/L) was prepared for each dye to be degraded (MeO, MB and RhB) and to each of these, 30% H_2O_2 (1.5 ml) was added in conjunction with CuO to enhance degradation efficiency by generating more free radical species in solution[33]. A mass (50 mg) of the catalyst (CuO) was then added to the above mixture and stirred in the dark for 15 minutes to establish an equilibrium prior to irradiation. The resultant mixture was then exposed to light from a 400 W Skylite mercury (Hg) bulb. The setup consisted of a rectangular box on which

the bulb was installed as illustrated in Figure 3.4. The top of the box was lined with aluminium foil to ensure that all dispersed light rays are reflected to the solution undergoing degradation. Small amounts of solution were then sampled at 25 minute intervals and analysed using a UV-vis spectrophotometer to determine their absorbance.

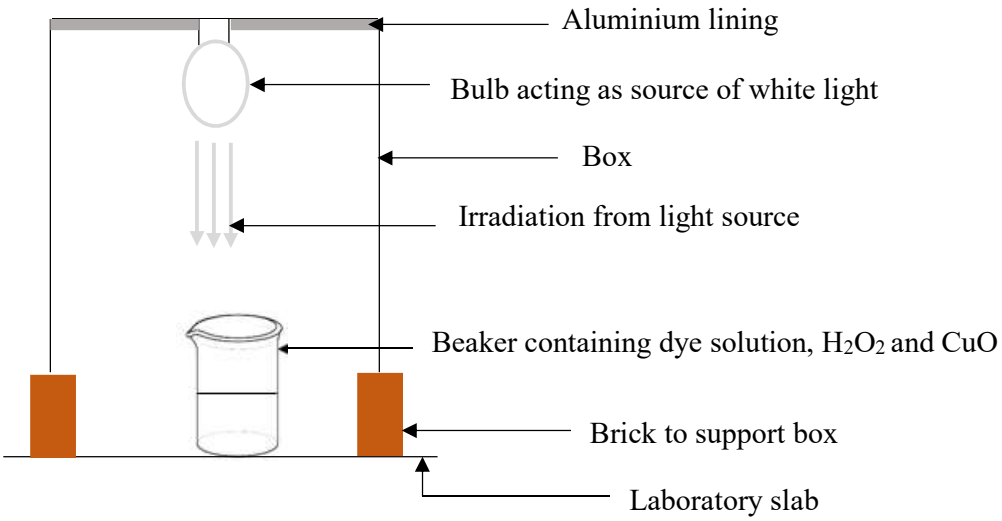

Figure 3.3: Setup for photocatalytic degradation of the dyes (MeO, MB, RhB) using CuO nanoparticles

CHAPTER FOUR

4.0 Results and Discussion

Three CuO samples were analysed using different characterisation techniques to determine their properties. The different samples were denoted as N60, S25 and N60 where:

- N60 represents CuO samples precipitated at 60°C from the $Cu(NO_3)_2.3H_2O$ precursor salt solution.
- S25 represents CuO samples precipitated at 25°C from the $CuSO_4.5H_2O$ precursor salt solution.
- S60 represents CuO samples precipitated at 60°C from the $CuSO_4.5H_2O$ precursor salt solution.

From literature, Cu^{2+} ions in solution are said to generally have a coordination number of six. This implied that at any point in time within the solution, each one of the Cu^{2+} ions is surrounded by six other molecules, atoms or ions. In this research whereby the solvent was water, six water molecules will arrange themselves around a central Cu^{2+} ion in a process called solvation. Because the solvent is water, this solvation process can also be termed hydration. However, on the basis of a model called the anionic coordinative polyhedral theoretical model[78], with the addition of NaOH and the consequent introduction of ^-OH ions in solution, the structure formed tends to exist as a complex whose ligands are ^-OH ions in solution, with four out of the six ligands being arranged in a square planar shape around the Cu^{2+} cation and two lying in its axis as illustrated in Figure 3.1. According to this model still, each complex is a building block or basic unit from which the growth of the crystal which is being formed (CuO in our case) begins. Within this $Cu(OH)_6^{4-}$ complex, the four ^-OH ligands which together make-

up the square planar figure have lower binding energies compared to the other two at the axis. This arises from the fact that the inter-planar distances between the four ligands in the square planar and the central Cu^{2+} ion are shorter than those for the two axial ^{-}OH ions. The shorter this distance, the stronger the bonds. The result is that the two axial ions are generally more easily dehydrated into CuO and therefore growth of the CuO crystal will be rapid in this axial direction[15].

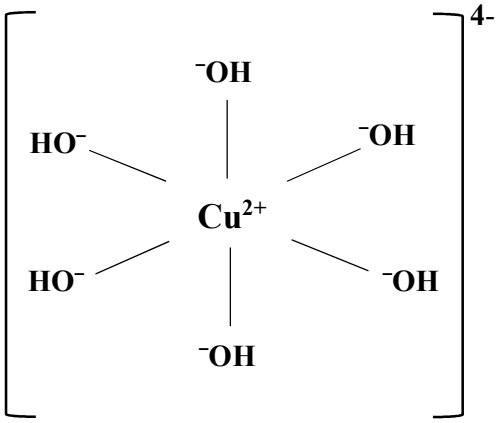

Figure 4.1: Structure of the $Cu(OH)_6^{4-}$ complex

The explanation above also gives us reason as to why the conversion of the $Cu(OH)_6^{4-}$ complex into CuO was much slower when NaOH was added to the copper precursor salt solution at 25 °C compared to when it was added at 60 °C. This is because at lower temperatures (25 °C), the ligand bonds are more stable compared to when synthesis is carried out at a high temperature (60 °C), which could result in the ligands forming hydrogen bonds with each other under such conditions, further stabilising the blue copper hydroxide complex. On the other hand (at higher temperatures) the heat energy supplied would break-down any hydrogen bonds present and inhibit the further formation of such and the ligand bonds will also be broken-down

(axial first) resulting in dehydration of the complex and formation of a CuO black precipitate[78].

4.1 X-Ray Diffraction (XRD)

The XRD patterns were compared to reference codes 01-089-5895, 01-070-6829 and 01-070-6831 for N60, S60 and S25 respectively and are shown in Figures 4.1 (a) and (b). Using the classical Scherrer equation for average crystallite size estimation, the particle sizes for the three samples were found to range from 12 – 13.5 nm with the change in size following the order S60 ~ S25 > N60.

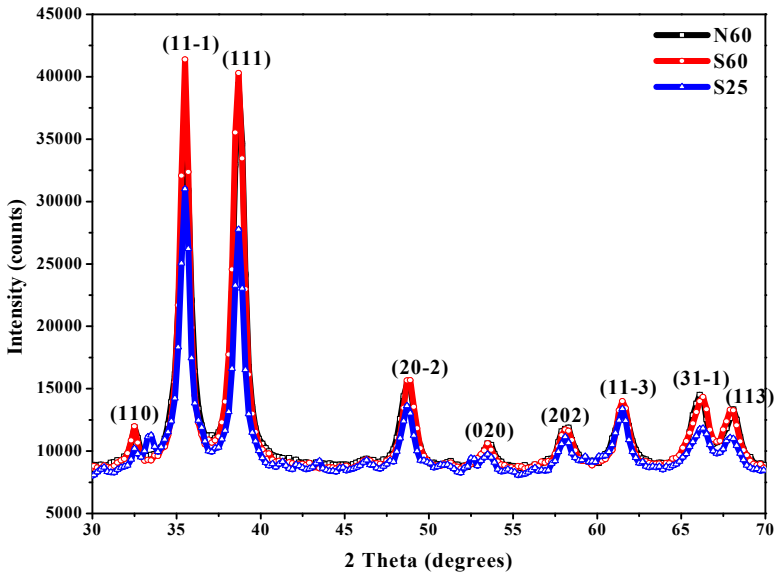

(a)

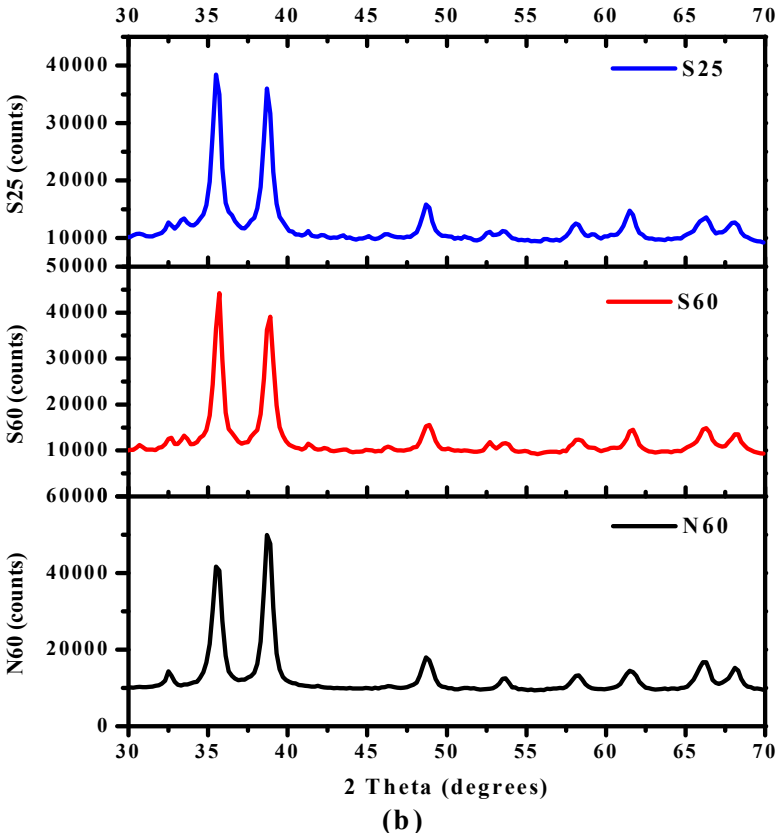

Figure 4.2 (a) XRD plot of the different CuO nanoparticles showing preferred growth planes of the particles, (b) Stacked XRD plots showing individual CuO sample profiles

According to the simple solution chemistry procedure put forward by Zhu et al.[15] for the synthesis of CuO nanoparticles, the nanoparticles which arose from a 60 °C NaOH adding temperature were found to have an estimated 15 nm crystallite size which is close enough to the 12 and 13.5 nm calculated for N60 and S60 respectively in this study. More so, despite the use of a different precursor salt ($CuSO_4.5H_2O$) instead of $Cu(NO_3)_2.3H_2O$ as starting material, the trend in increasing particle size with increasing NaOH adding temperature was still observed between the S25 and S60 nanoparticle samples. This study therefore found that whether $Cu(NO_3)_2.3H_2O$ or $CuSO_4.5H_2O$ is used as precursor salt, there will be no significant

difference for trends in crystallite size with NaOH adding temperature observed amongst CuO nanoparticles originating from the same precursor salt.

Because of the larger size of the sulphate ion compared to its smaller nitrate counterparts in solution, it could be suggested that it shields the Cu^{2+} ions more from interacting with the water molecules to form the $Cu(OH)_6^{4-}$ complex (Figure 3.1). This may result in shorter and stronger Cu-O bonds from the nitrate precursor and a corresponding smaller crystallite size compared to those originating from their sulphate counterparts as is observed in this research[78].

From the plot in Figure 4.1 (a) it can be observed that for all three CuO samples synthesised, the most densely packed planes (preferred plane orientation for particle growth) are the {111}. This can be explained by the fact that CuO's maintains most of its backbone structure which originates from a fundamental copper metal crystal lattice[33] in which the{111} planes are the most densely packed.

Figure 4.2 (a), (b) and (c) show the XRD models of the different samples comparing the experimental values of CuO to the calculated (theoretical) values. The difference between the two values for each sample is minimal, confirming that CuO nanoparticles were indeed synthesised.

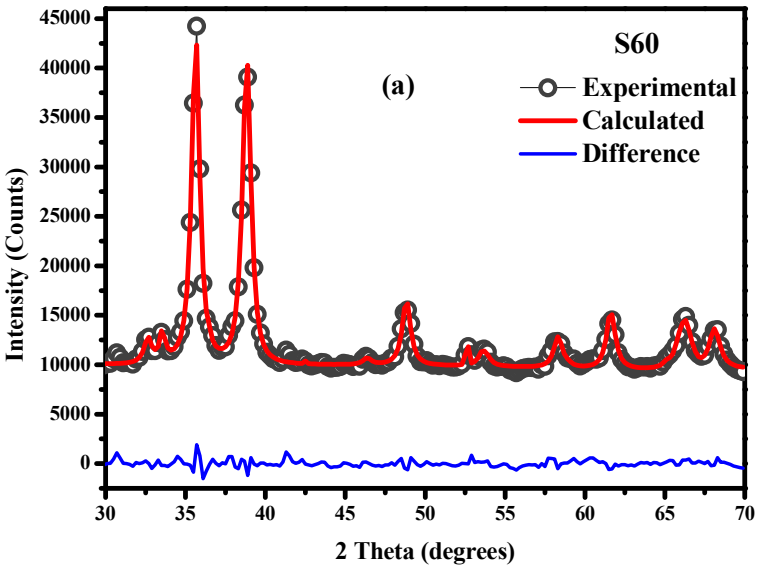

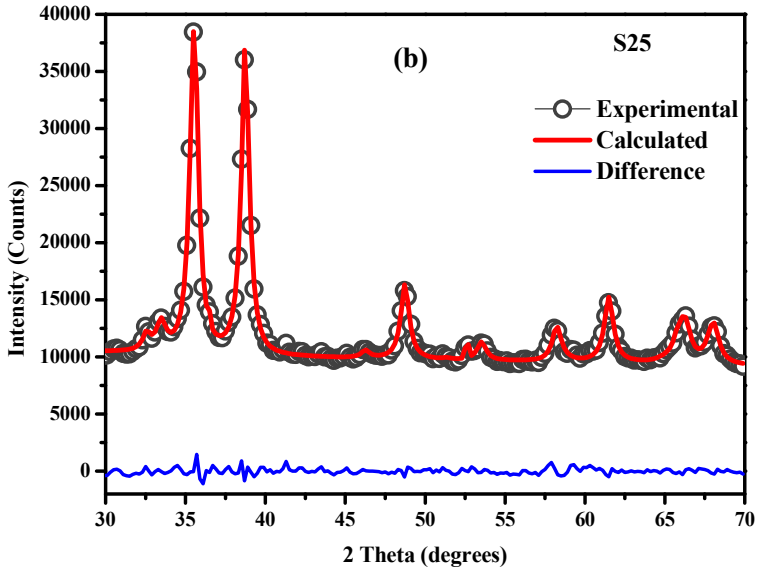

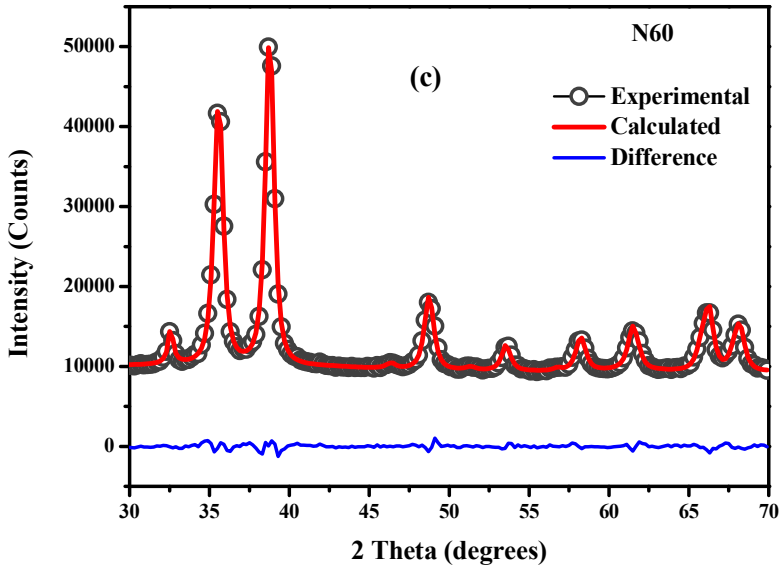

Figure 4.3: Modelled XRD patterns for (a) S60, (b0 S25 and (c) N60

4.2 UV-Vis Spectroscopy

The absorbance curves for the three CuO samples are shown in Figure 4.3. The curves show broad shoulders from 255 nm to 450 nm. Given that the wavelength of absorption (and not the intensity) was the point of focus for this measurement, the amount of each sample mixed in solution and used for the absorbance measurement was taken at random. This is thought to have resulted in the differences in absorbance intensity observed.

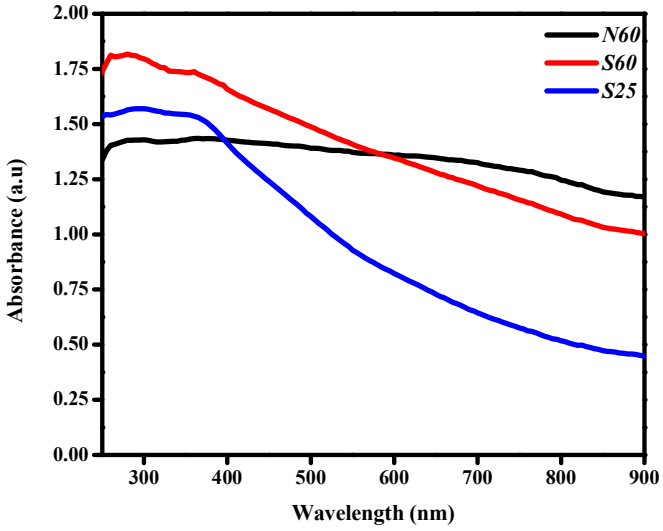

Figure 4.4: Absorbance values for the synthesised CuO samples

From the tauc plots for each sample, the band gap energies of the three samples were estimated to range from 2.12 – 2.4 eV. This suggested that the synthesised nanoparticles were most likely to absorb photons within the visible range of the electromagnetic spectrum. The change in bandgap followed the order S60 ~ S25 < N60. Following the quantum size effect phenomenon observed in CuO[35], [36] whereby bandgap energy increases with decreasing crystallite size, the trend in bandgap energies was in agreement with the XRD data obtained during this research. N60 having the smallest average crystallite size should therefore have been expected to have the highest bandgap as was observed in this study. Similar absorbance profiles with corresponding bandgap energies have been recorded in literature for CuO nanoparticles of about the same size[30].

4.3 FTIR

The FTIR spectrum for the synthesised CuO nanoparticles is shown in Figure 4.4. The peaks at 3475, 2927 and 3390 cm^{-1} correspond to OH stretching vibrations from water molecules

adhered to the surface of the nanoparticles. The peaks at 1636 cm^{-1} and 1644 cm^{-1} correspond to a Cu-O bond vibrational mode[79]. The peaks at 482, 498, 595 and 603 cm^{-1} can be assigned to CuO vibrational modes[79]–[81]. All peaks from 482 to 1364 cm^{-1} can be assigned to CuO vibrational modes[82].These peaks therefore confirm the presence of CuO nanoparticles.

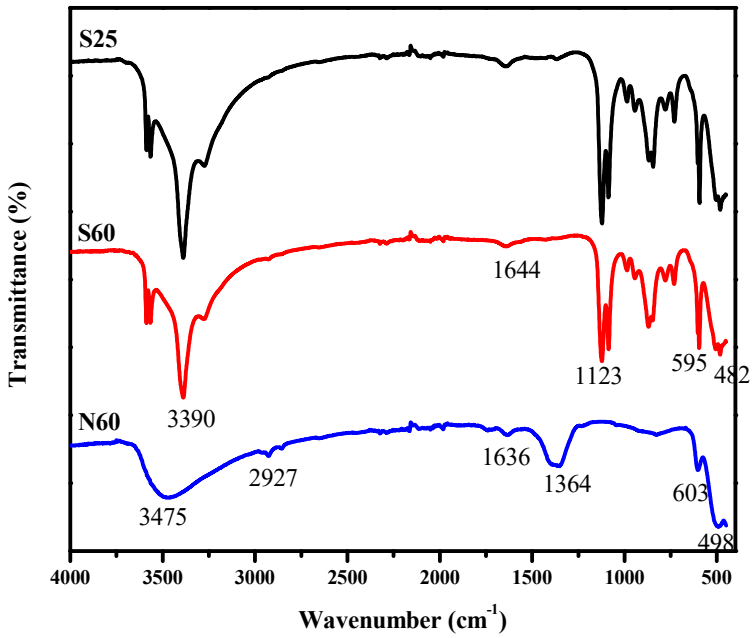

Figure 4.5: FTIR plot for the synthesised CuO samples

4.4 Scanning Electron Microscopy (SEM)

Figure 4.5 shows pictures of SEM analysis of the synthesised CuO nanoparticles. The SEM shows agglomerates of the CuO nanoparticles. The surface of nanoparticles have a hairy appearance which is indicative of the presence of finer (smaller) particles which together makeup the bulk mass which can be observed under the SEM.

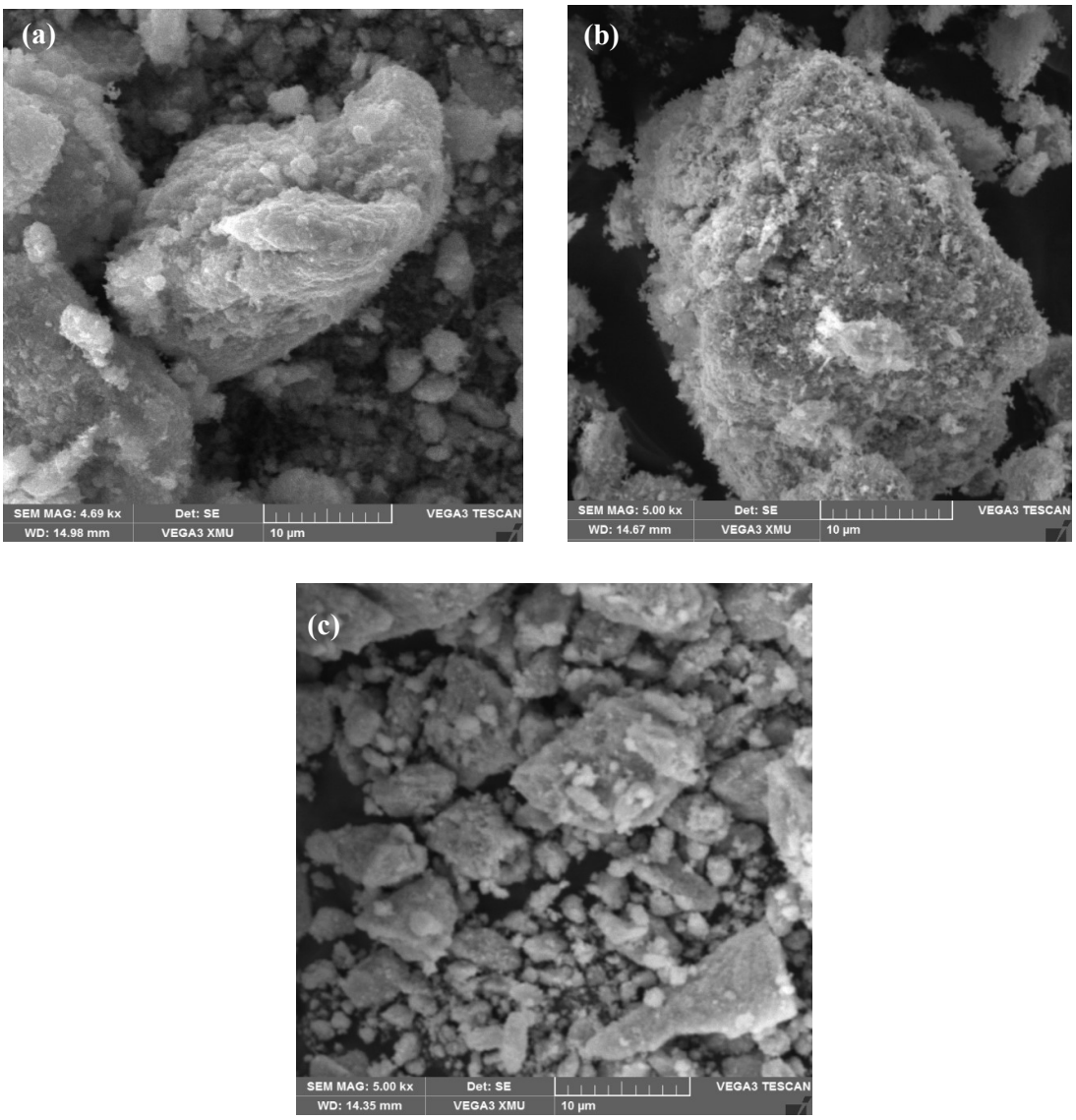

Figure 4.6: SEM images of (a) S60, (b) S25 and (c) N60

4.5 Energy Dispersive X-Ray Spectroscopy (EDX)

Figures 4.6 – 4.8 (a) and (b) show the EDX plots and atomic distribution for S60, S25 and N60, respectively. Except for N60 (which has a higher O ratio arising from an external source and is not a cause for concern), the weight percent (wt %) and atom percent (at %) indicate clearly for S60 and S25 that the atoms exist in the mole ratio 1:1 which is the case in the compound CuO. This therefore further confirmed that the synthesised particles were CuO nanoparticles.

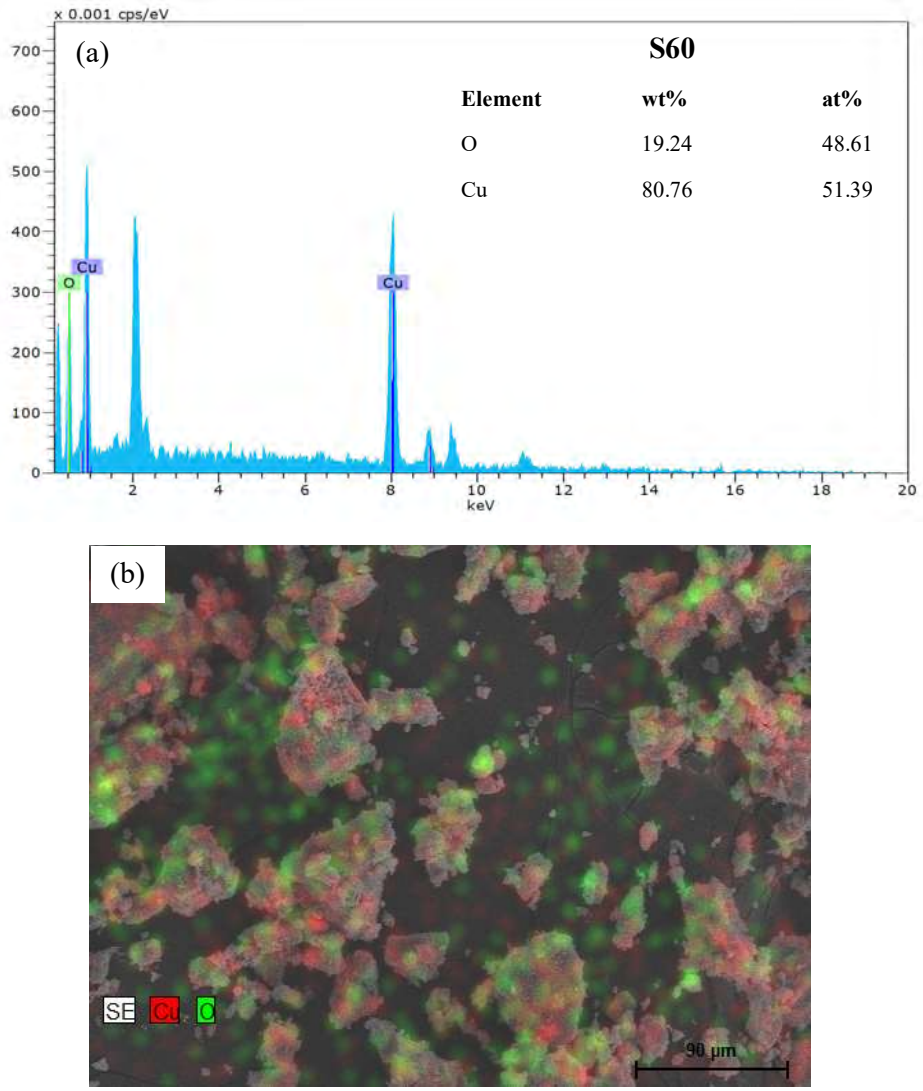

Figure 4.7: (a) EDX spectrum and (b) Picture showing atomic distribution of Cu and O in S60 sample

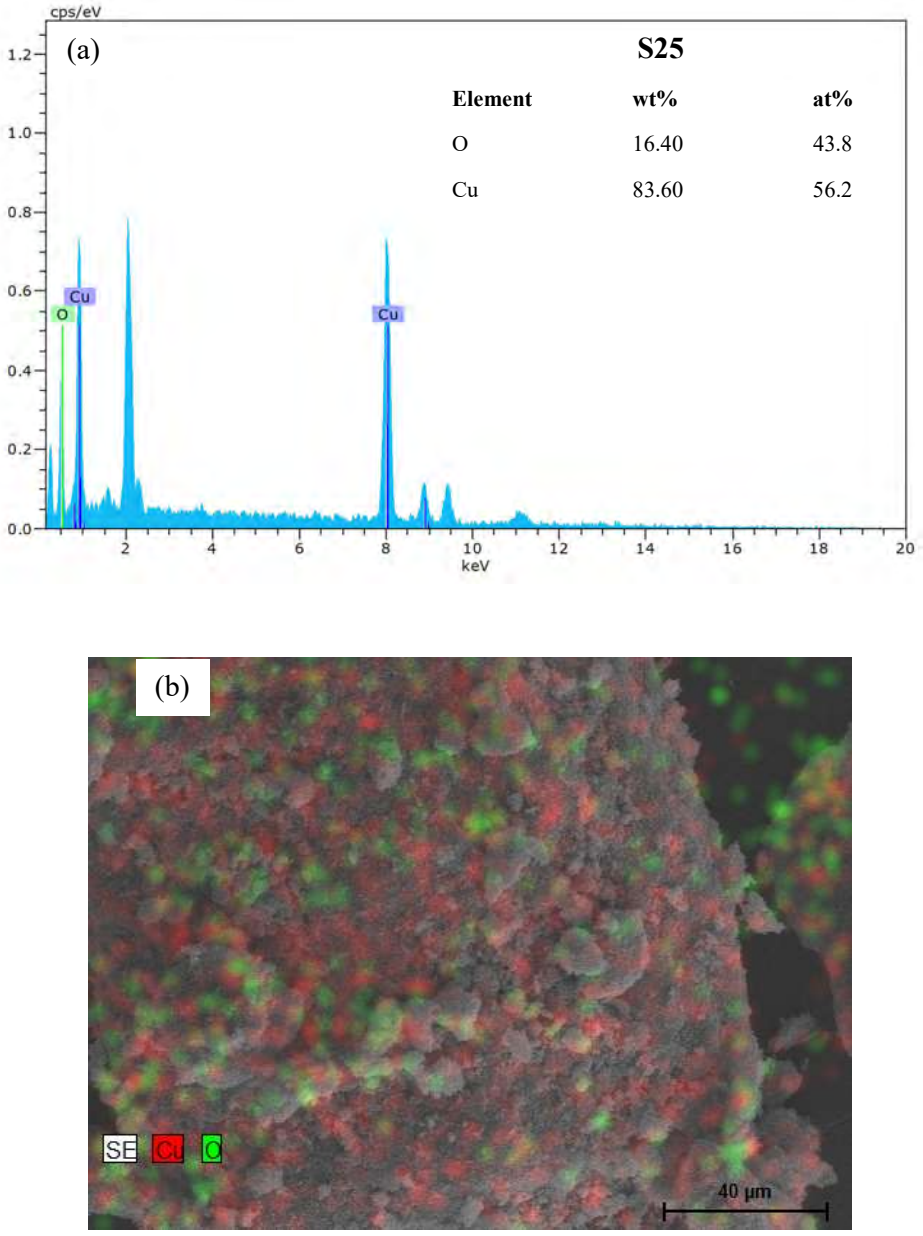

Figure 4.8: (a) EDX spectrum and (b) Picture showing atomic distribution of Cu and O in S25 sample

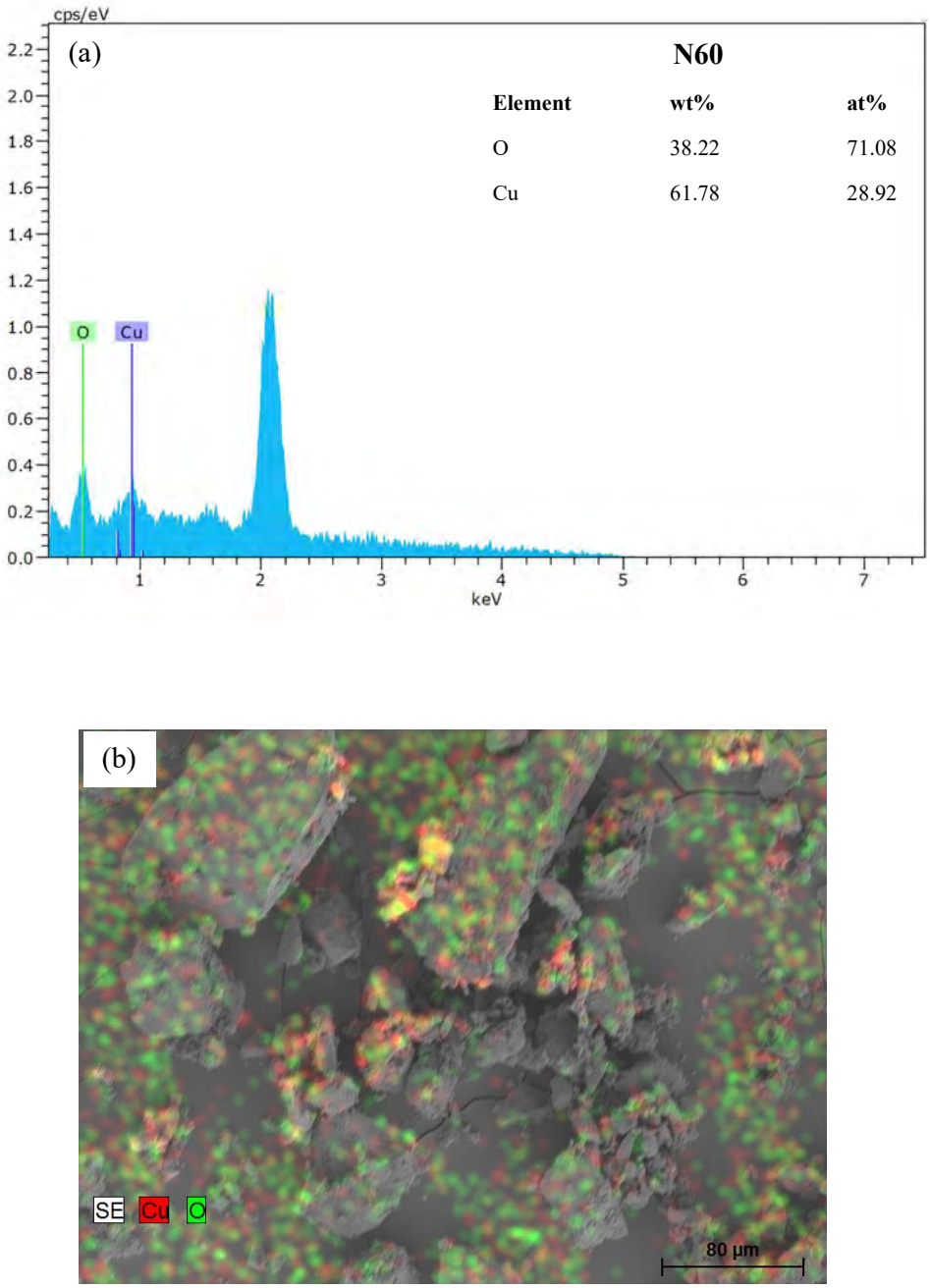

Figure 4.9: (a) EDX spectrum and (b) Picture showing atomic distribution of Cu and O in N60 sample

4.6 Brunauer–Emmett–Teller (BET) Surface Analysis

4.6.1 Adsorption Isotherms

4.6.1.1 Carbon dioxide (CO_2) adsorption isotherms

The carbon dioxide (CO_2) adsorption isotherms are shown in Figures 4.9 (a), (b), (c) and (d) for S60, S25, N60 and a combination of all three respectively. All three samples portrayed a characteristic Type I isotherm profile according to the IUPAC classification of adsorption isotherms for gas-solid equilibria[83]. This profile describes adsorption occurring on an adsorbent with very small (microporous) pores. Figure 4.8 (d) shows that N60 had the highest adsorption values compared to S60 and S25 indicating that N60 had many more micro pores than S60 and S25 and has a higher affinity for the adsorbent.

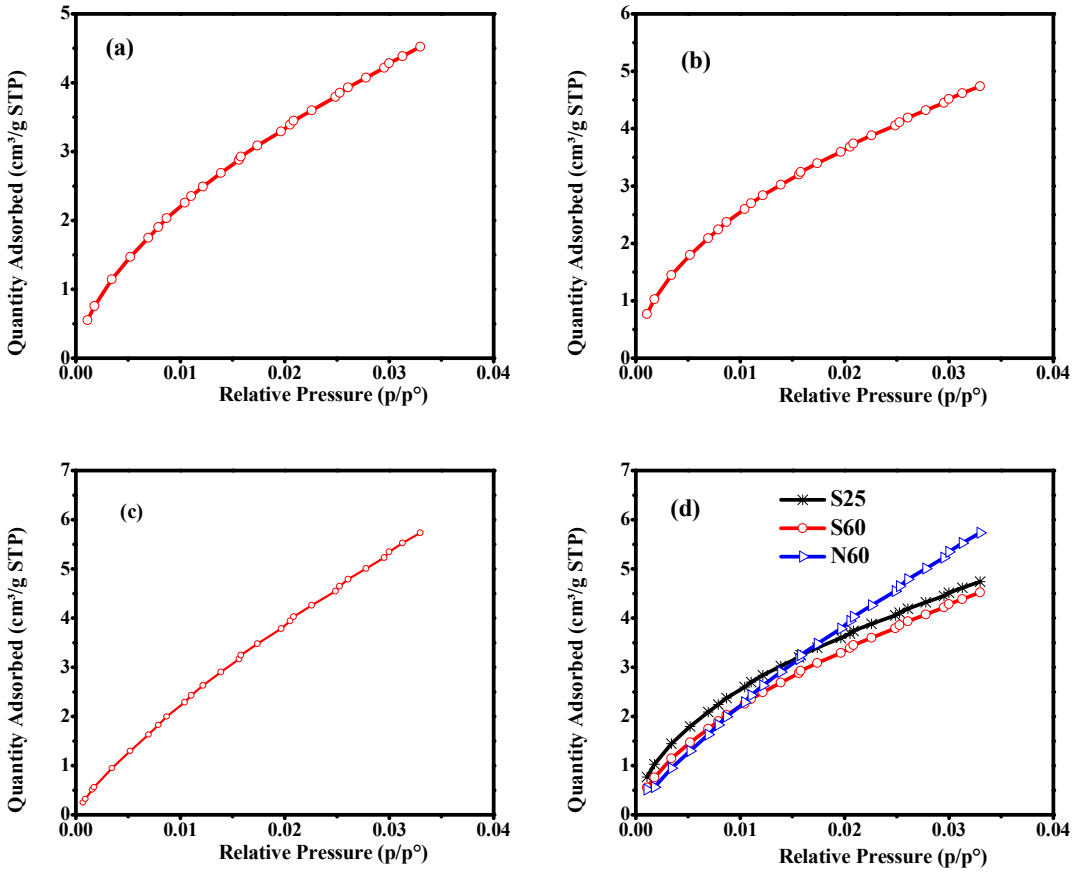

Figure 4.10: CO_2 adsorption isotherm for (a) S60, (b) S25, (c) N60 and (d) S60, S25 and N60 combined

4.6.1.2 Nitrogen (N_2) adsorption isotherms

Brunauer et al. conducted a study which showed that it is convenient to separate the classification of adsorption isotherms into two parts made up of five adsorption isotherms; one at low relative pressures (Type A and B, $0 < P/P_o < 0.3$) as shown in Figure 4.10 and the other at higher pressures as shown in Figure 4.11. This comes from the suggestion that the isotherms will behave differently at these two points owing to the differences in adsorbate-adsorbent interactions which characterise the two regions[84].

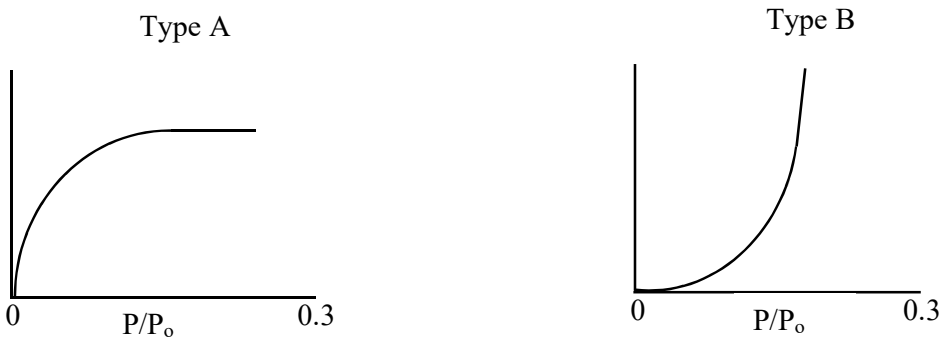

Figure 4.11: Graphs showing initial behaviours of adsorption isotherms (low relative vapour pressures). Adapted from[84]

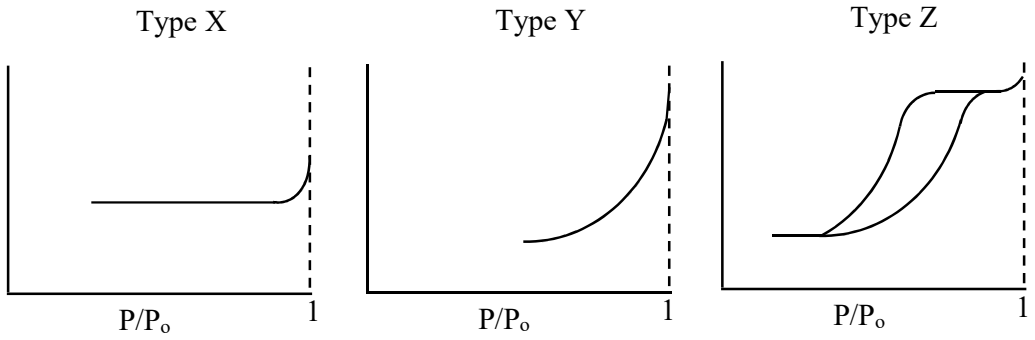

Figure 4.12: Graphs showing behaviour of adsorption isotherms at high pressures. Adapted from[84]

The study further states that Type A profiles are characteristic of microporous adsorbents with strong adsorbate-adsorbent interactions. It also suggests that surface area calculations are done from this section of the isotherm. This agrees with our findings stated earlier in section 4.6.1.1 in relation to Figure 4.8 where the relative pressures only went up to 0.04. Type B describes a situation where the adsorbate-adsorbate interactions are very significant and in some cases equal to the adsorbate-adsorbent interactions thereby influencing any calculations made from this section of the isotherm significantly. In type X profiles the isotherm is almost unaffected by the increase in pressure while in Type Y there exists a desorption curve which is not visible simply because it follows the same profile as the adsorption curve. This implies the adsorbed gas is desorbed without any retention. Type Z describes a profile in which the desorption curve does not follow the adsorption profile until further down at low pressures where they reunite. This is due to the fact that some of the adsorbed gas particles are temporarily retained and once they are released at lower pressures, the desorption and adsorption curves meet again[84].

From the study discussed above, a nitrogen (N_2) adsorption study was carried out on S60 and N60. This assisted in the classification of the isotherm for region of higher relative pressure. The N_2 adsorption profiles which were obtained are shown in Figure 4.12 (a) and (b) for S60 and N60 respectively.

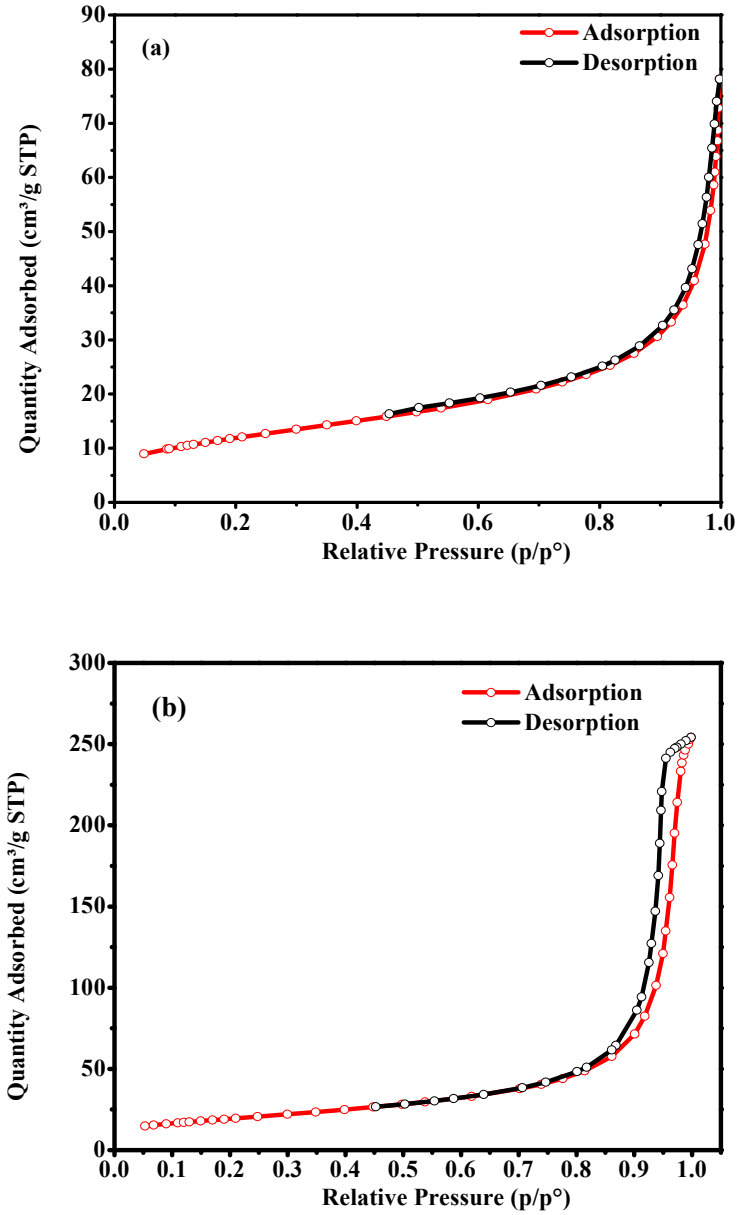

Figure 4.13: N_2 adsorption isotherm of (a) S60 and (b) N60

At higher pressures ($P/P_o = 0.3$) in S60, adsorption increases with increasing pressure but the effect of the interaction of the gas molecules with the external surface overshadows that of any micro pores that might exist in this region. The result is that there is no retention of adsorbate within pores and desorption follows the same pathway as adsorption , giving rise to the

Brunauer Type Y profile (Figure 4.10) which corresponds to IUPAC Type III adsorption isotherm. This indicated that within this sample, in addition to the micro pores identified by the isotherms in Figure 4.9 which make up the majority, there also existed few particles with large (macro) pores with weak adsorbate-adsorbent interactions at their surfaces[83]. While it is not uncommon to find one sample with multimodal (micro, meso, macro) pore sizes is not unusual and this type of adsorption profile also suggest the presence of aggregated nanoparticles[85].

N60 also showed an increase in adsorption with pressure at higher pressures but desorption did not follow the same path as adsorption, resulting in the hysteresis loop observed in Figure 4.11 (b). This is indicative of the fact that there was some degree of retention of the adsorbate on the adsorbent until later at lower pressures where they were totally released from the adsorbent's surface. This resulted in Type Z, Brunauer classification profile which is identical to IUPAC Type IV profile and characteristic of mesoporous particles[83], [84].

Despite the higher molecular weight of CO_2 compared to N_2, the former has a smaller kinetic diameter which may enable it interact better with microporous materials than N_2[86]. This might suggest that it may be able to interact better with micro pores thereby revealing a more defined and accurate profile at lower pressure, where micro pores are most likely identified (Figure 4.9). N_2, having the larger kinetic diameter on the other hand may be able to define a more accurate profile at higher pressures where larger pore size are most likely identified.

4.6.2 BET Surface Area and Pore Size

The relationship between BET surface area and pore size for each of the synthesised CuO nanoparticles is shown in Figure 4.13. The BET surface area is seen to decrease from 28.4 m^2/g in S60 to 26.8 m^2/g in S25 and that of N60 being the highest (49.3 m^2/g). This implies that the

CuO particles synthesised from the copper nitrate precursor salt generally have a higher BET surface area than their counterparts synthesised from the sulphate precursor. This could be due to the fact that on precipitating, nitrates generally form more colloidal solutions than sulphates. This would mean the sulphates will have a greater tendency to coagulate or form agglomerates on precipitating thereby resulting in larger particles than their nitrate counterparts as can be seen from the SEM. The recorded surface area values were also noted to be high compared to some observed in literature for other CuO nanoparticles. For example, Zaman et al.[74]recorded an 8.4 m^2/g maximum for surface area while Sasikala et al. [7] recorded 1.82 m^2/g (for bare CuO) and 5.54 m^2/g (for cerium loaded CuO).

The trend in pore sizes for each CuO sample progresses in the opposite sense whereby the CuO particles originating from the sulphate precursor, tend to have larger pore sizes compared to their N60 counterpart. This is difference could have arisen from the differences in porosity due to internal space of the samples[85] where the more closely packed the molecules are within the crystal lattice, the smaller the intermolecular spaces and the smaller the average crystallite size.

The high surface area difference despite the low crystallite size difference between the CuO nanoparticles originating from sulphates and nitrates can be accounted for by the fact that sulphates are more likely to form agglomerated precipitates than nitrates leading to a great reduction in their surface sites (pores) available (exposed) for interaction with an adsorbate.

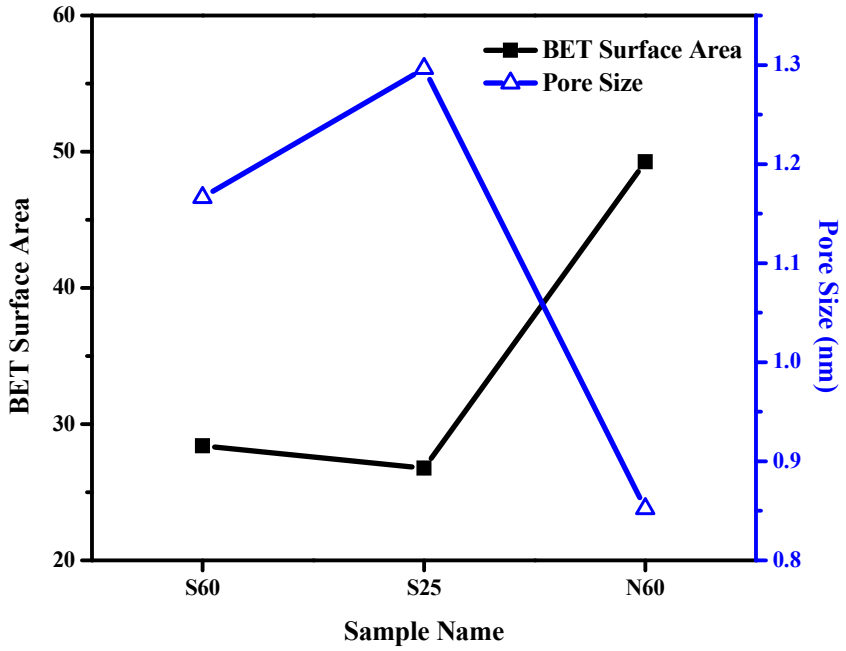

Figure 4.14: Plot showing relationship between BET surface area and micro pore size for the synthesised CuO nanoparticles

4.6.3 BET Surface Area and Pore Volume

Figure 4.14 shows the trends and relationships between the BET surface areas and pore volumes of the different CuO nanoparticles synthesised. The plot shows that the pore volume is directly related to the BET surface area as would be expected. This is because for a given material, a decrease in surface area is synonymous to taking away part of the material surface, and therefore taking away the pores on that part of the material with the removed piece and vice versa. As such the two properties follow the same trend for all three CuO samples. The values for the properties of the S60 and S25 samples are only slightly different despite the difference in NaOH adding temperature. This could be the effect of the tendency of S60 and S25 to agglomerate (see Section 4.6.2), thereby reducing the overall available surface area and corresponding pore space on the surfaces of these agglomerated nanoparticles.

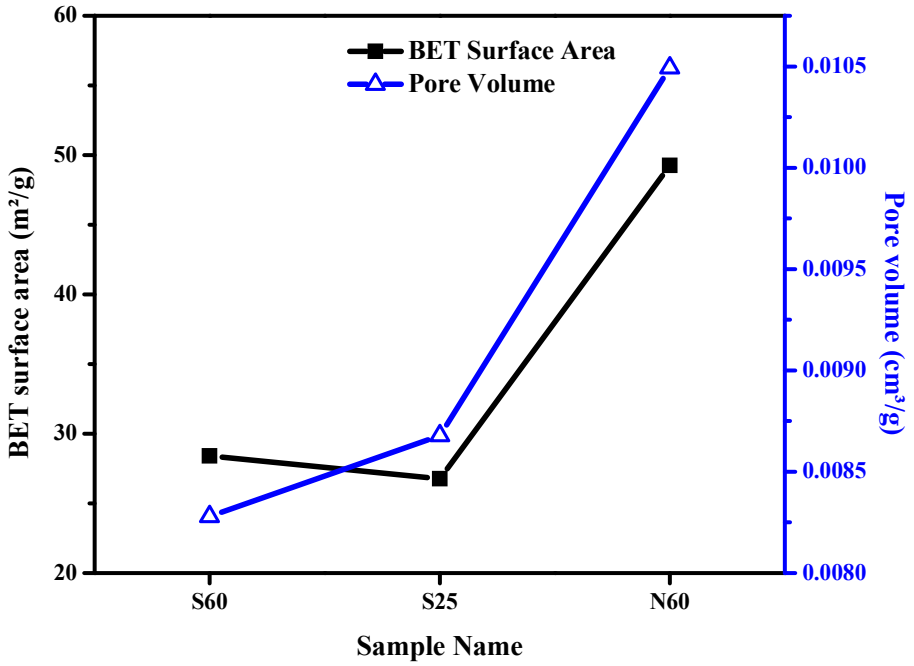

Figure 4.15: Plot showing the relationship between BET surface area and pore volume for the synthesised CuO nanoparticles

4.6.4 Micro pore Surface Area and Pore Volume

The micro pore surface area and pore volume trends are shown in Figure 4.15. They have similar relationships as the BET surface area and pore volume as discussed in Section 4.6.3.

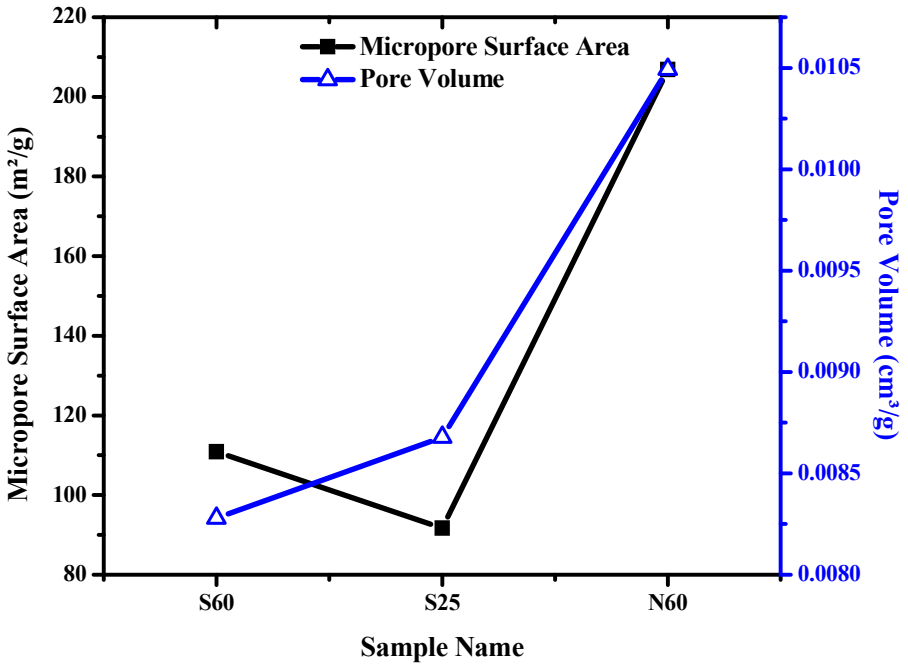

Figure 4.16: Plot showing relationship between micro pore surface area and pore volume of the synthesised CuO nanoparticles

4.7 Photocatalysis

4.7.1 Visible Light Degradation

A summary of the degradation efficiency of each of the synthesised CuO species in the respective dyes is shown in Figure 4.16 while the absorbance (degradation) plots for the individual samples in each dye (MeO, MB and RhB) in the presence of the visible light source are shown in Figures 4.17, 4.18 and 4.19. A general decrease in the absorbance (concentration) of dye is observed with time owing to the continuous production and consumption of •OH radicals (in the breakdown of the dye, Figure 2.1). It can be seen from Figure 4.16 that within 100 minutes each CuO sample was able to degrade all three dyes up to a minimum 85 % (in MeO) and a maximum 99 % (in RhB). These percentages were achieved within a shorter time

interval than some degradation studies in literature did. For instance, Zaman et al.[74] and Sasikala et al.[6] cited earlier in section 4.6.2 while comparing BET surface areas, both recorded a 95 % and 98 % maximum degradation respectively only after 5 hours of degradation.

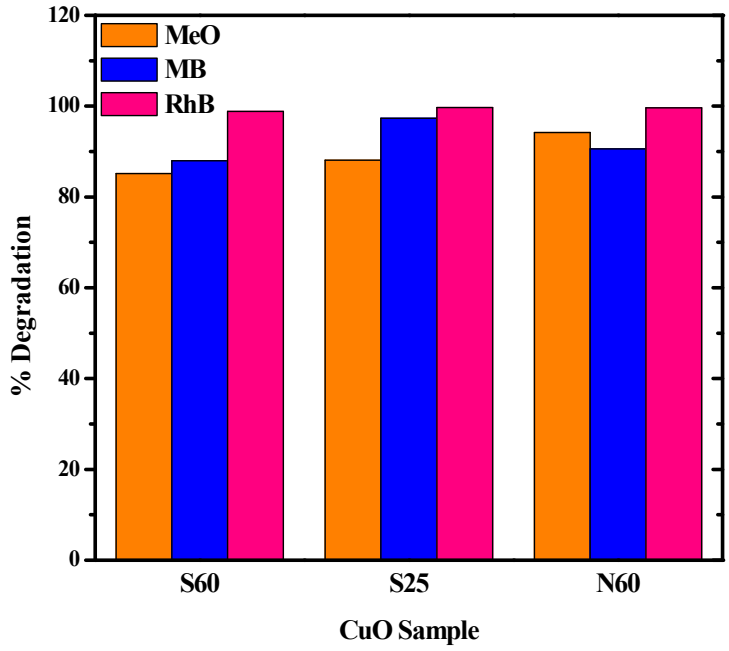

Figure 4.17: Summary of average percentage degradation for each sample in each dye

In each case, N60 proved to unfailingly have a very high degradation efficiency hypothesised to be directly associated with the highest BET surface area and smallest particle size recorded for N60 samples when compared to the other two samples (See section 4.6). Generally, all the classes of dye responded well to the photocatalytic degradation regime applied in the presence of the synthesised CuO nanoparticles, with RhB having the highest degradation percentages per CuO sample at the end of the 100 minutes.

4.7.2 Changes in dye concentration with time

The changes in concentration of the dyes during the degradation process are shown in Figure 4.17 and have been expressed as percentages. A general decrease in the amount of dye in solution with time of exposure to the light source can be observed across all three dyes. This can be explained by the fact that exposure of the dyes to the photocatalytic system leads to their degradation facilitated by •OH radicals in solution which ensues continuously as long as the catalyst is exposed to the visible light. Carbon dioxide and water are the main end products of this breakdown with other elements present ending up as inorganic ions in solution (See Figure 2.1). The percentage of the residual dye was calculated following Equation 4.1 owing to the fact that the change in amount of dye (concentration) with time is directly proportional to the change in absorbance as shown in Equation 4.2. The same was used to calculate the percentage degradation of the dye over time for the three synthesised CuO samples.

$$\% \text{ Dye remaining in solution} = (A_t / A_0) \times 100\% \quad 4.1$$

$$(A_0 - A_t) / A_0 = (C_0 - C_t) / C_0 \quad 4.2$$

Where A_0 = Absorbance after 0 minutes of degradation

A_t = Absorbance after t minutes of degradation

C_0 = Concentration after 0 minutes of degradation

C_t = Concentration after t minutes of degradation

Methyl Orange (MeO)

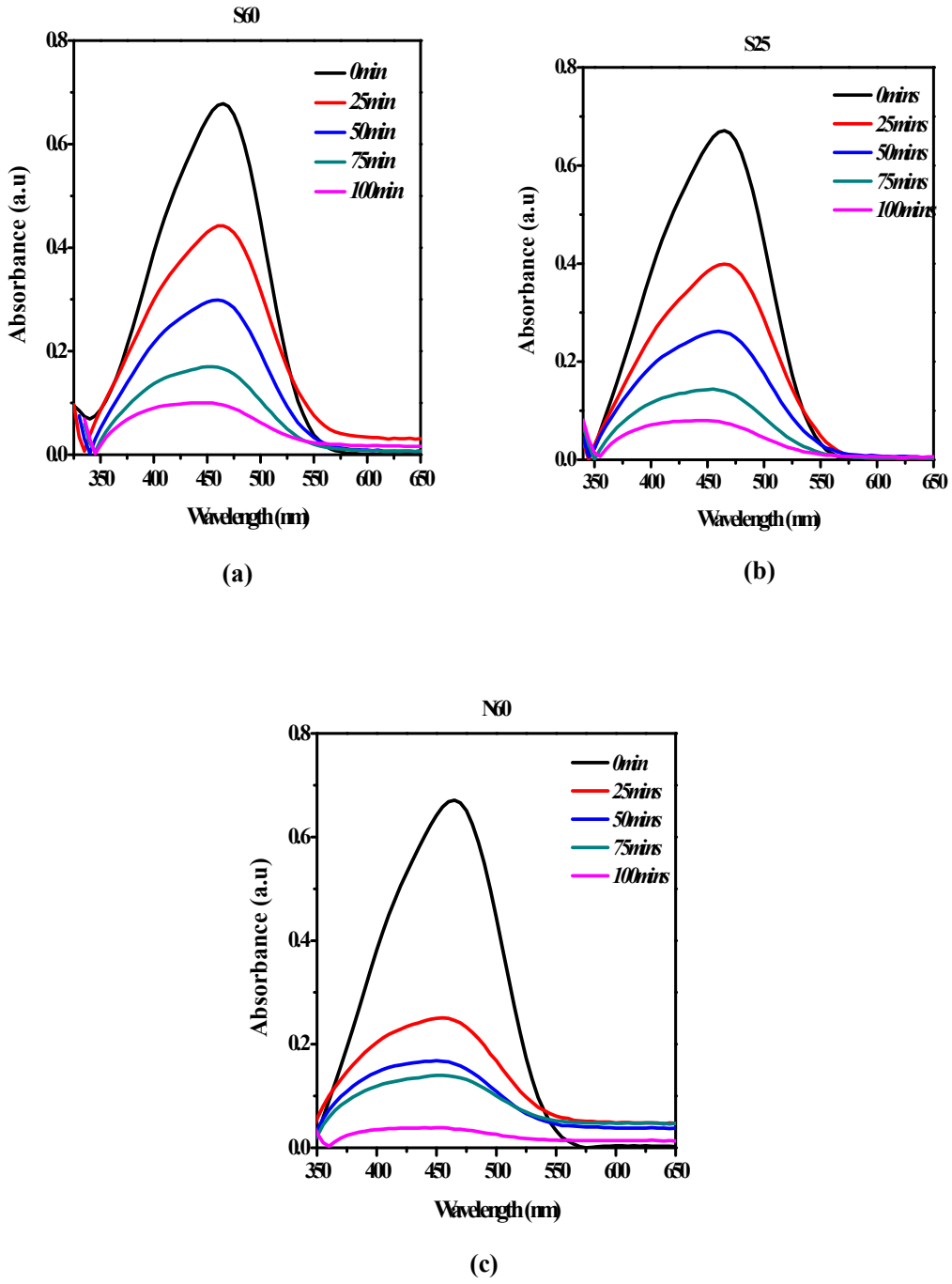

Figure 4.18: Absorbance curves for the degradation of MeO dye using S60, S25, N60

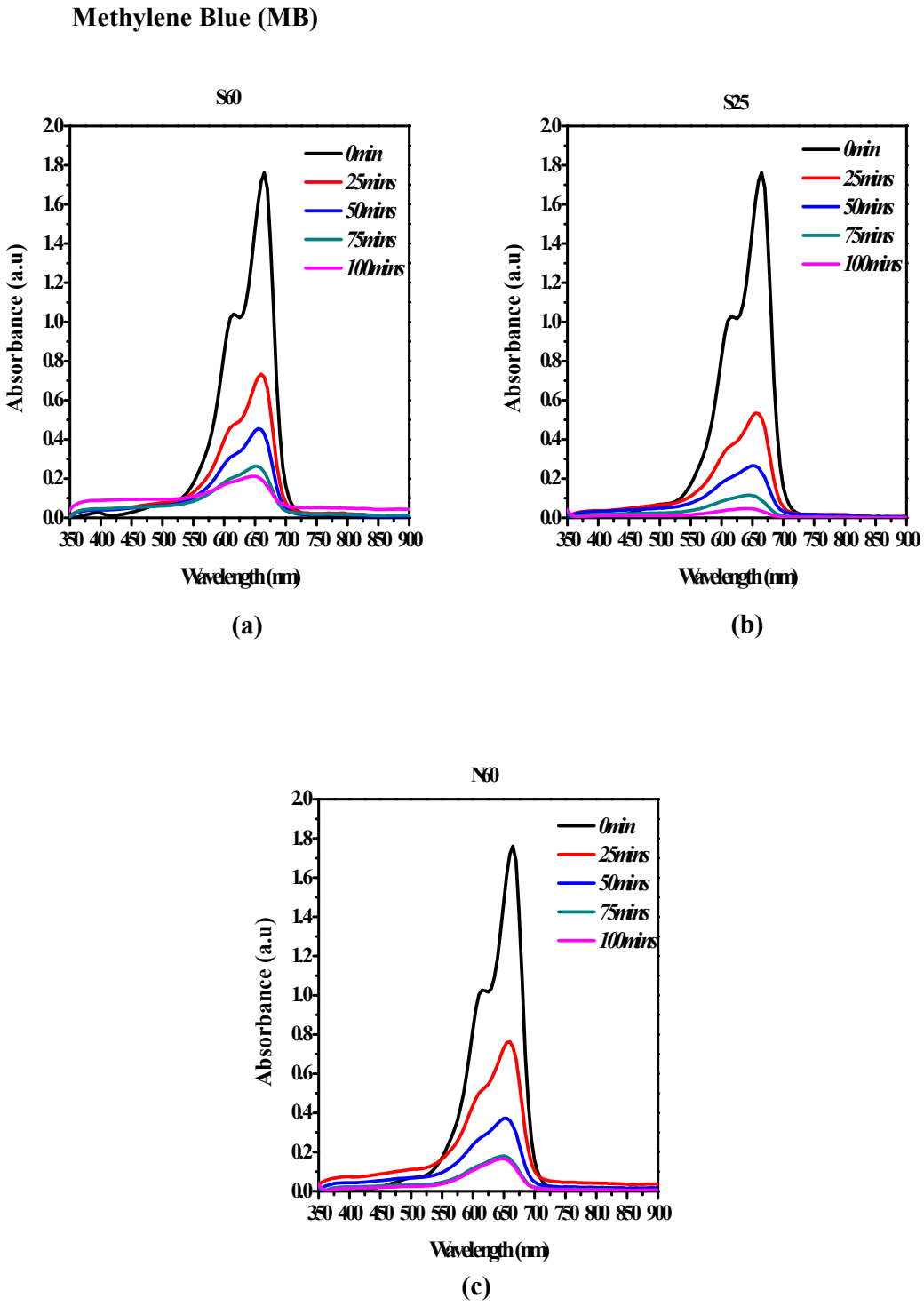

Figure 4.19: Absorbance curves for the degradation of MB dye using (a)S60, (b)S25 and (c)N60

Rhodamine B (RhB)

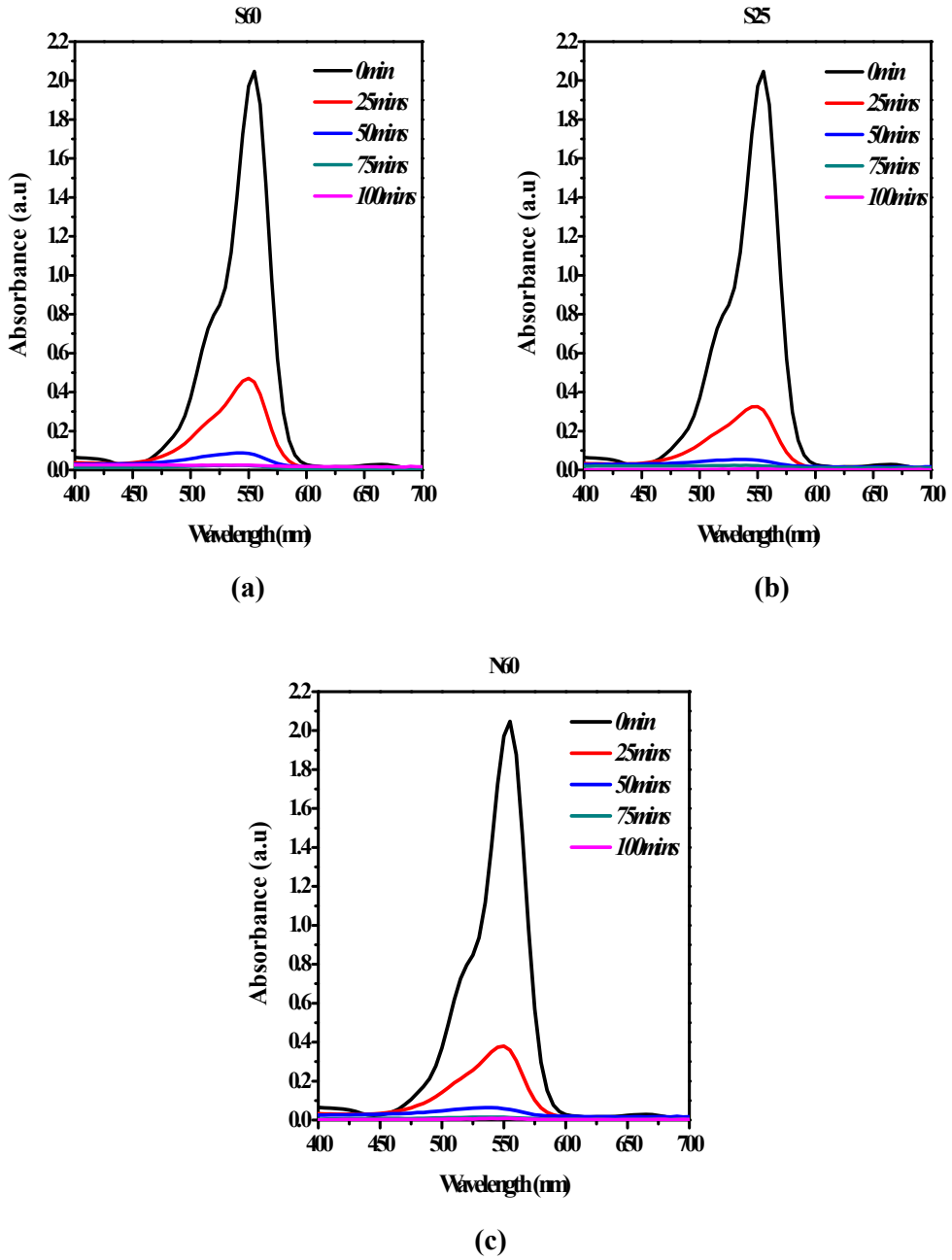

Figure 4.20: Absorbance curves for the degradation of RhB dye using (a)S60, (b)S25 and (c)N60

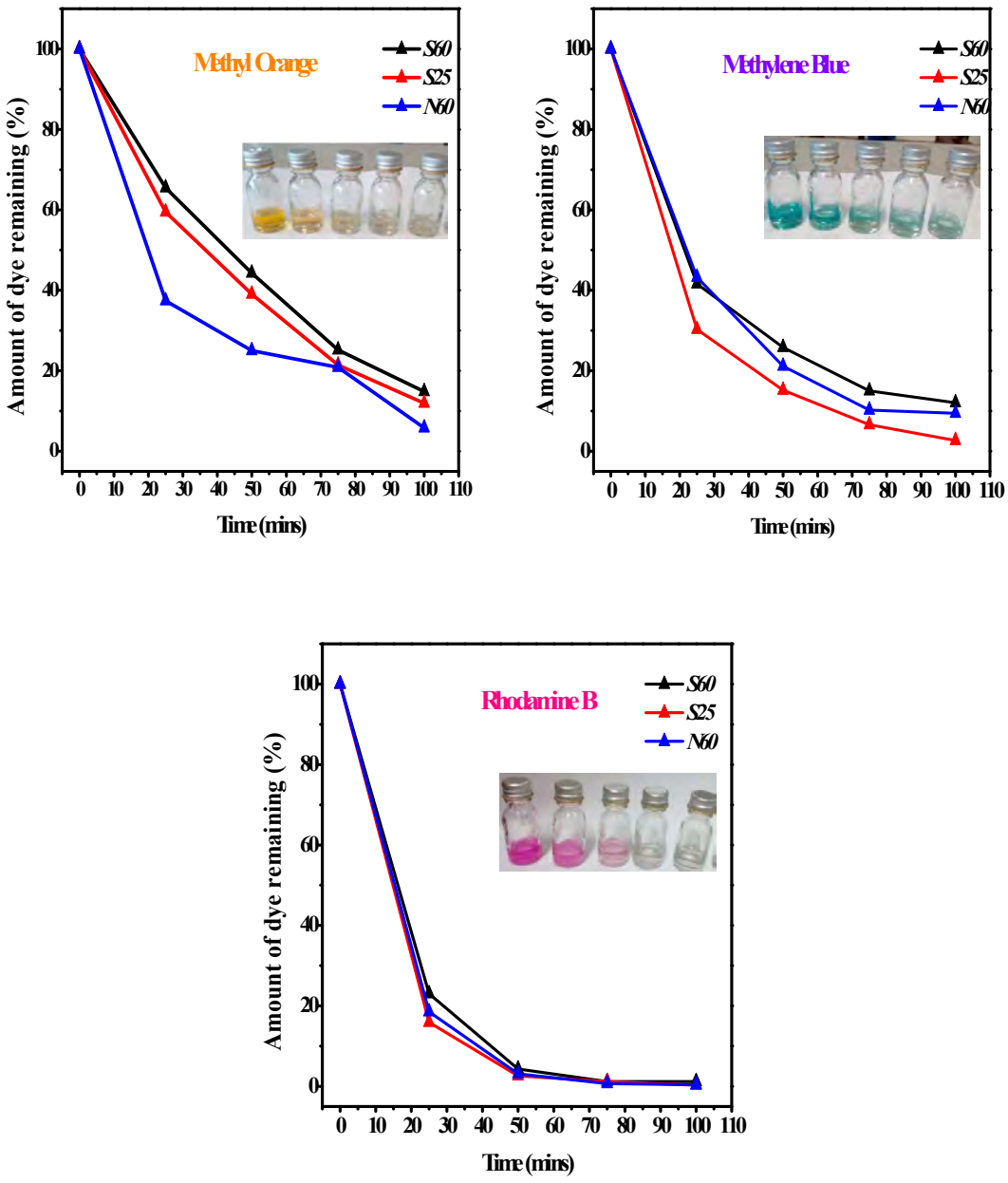

Figure 4.21: Plots showing change in concentration of dye (expressed in percentages) with time for MeO, MB and RhB

4.8 Characterisation Summary Report

Table 1: Summary of the characterisation data for the synthesised CuO nanoparticle samples

Sample Name	Particle Size (nm)	Band Gap (eV)	BET Surface Area (m^2/g)	Micropore Surface Area (m^2/g)	Pore Size (nm)	Pore Volume (cm^3/g)	Average % Degradation (over all dyes)
S60	13.5	2.12	28.4	110.9	1.2	0.0083	90.7
S25	13	2.11	26.8	91.7	1.3	0.0087	95
N60	12	2.4	49.3	206.9	0.9	0.0105	95

CHAPTER FIVE

5.0 Conclusion and Recommendations

From the results, CuO nanoparticles of different sizes were synthesised successfully from two different copper precursor salts, using a simple solution method without the use of surfactant. The synthesised particles were successfully characterised and found to have band gaps ranging from 2.11 eV to 2.14 eV and multimodal pore sizes. Their BET surface areas were 26.8 m^2/g, 28.4 m^2/g and 49.3 m^2/g and were found to be relatively higher compared to those in cited literature (See section 4.6.2). The nanoparticles were used to degrade three organic dyes; MeO, MB and RhB. From the 85 % overall minimum and 99 % overall maximum degradation value after 100 minutes, it can be concluded that the synthesised CuO nanoparticles can be suitable for the photocatalytic degradation of azo and rhodamine dyes with a slightly quicker or more effective degradation potential on rhodamine dyes. The N60 sample, with the highest BET and micro pore surface areas performed consistently better, by facilitating the degradation of all the dyes assessed compared to the other catalyst samples within the same time interval. It was therefore the preferred photocatalyst in terms of its consistent efficiency across both dye classes.

This research pointed out that following this method of synthesis, nitrate precursors would be a better choice over sulphates for the synthesis of CuO nanoparticles for surface applications. This is because the nanoparticles resulting from the nitrate precursors exhibit very high (almost double) surface areas and pore volumes compared to those originating from the sulphate precursors.

The results from this research suggest that the synthesised CuO nanoparticles could be suitable for wastewater treatment. Future research can be carried out to investigate the recyclability of the CuO nanoparticles, effect of pH on degradation and the kinetics of the degradation process. Emphasis can be laid on the CuO nanoparticles arising from the nitrate precursor salt, given their visible efficiency in this research.

REFERENCES

[1] P. B. S. Ratna, 'Pollution due to synthetic dyes toxicity & carcinogenicity studies and remediation', *Int. J. Environ. Sci.*, vol. 3, no. 3, pp. 940–955, 2012.

[2] B. D. C. Ventura-camargo and M. A. Marin-morales, 'Azo Dyes : Characterization and Toxicity – A Review', *Text. Light Ind. Sci. Technol. 2(2)*, vol. 2, no. 2, pp. 85–103, 2013.

[3] E. Concerns, 'The Environmental, Health and Economic Impacts of Textile Azo Dyes', *House Parliam. Sci. Technol.*, pp. 1–5, 2013.

[4] A. Majcen-Le Marechal, Y. M. Slokar, and T. Taufer, 'Decoloration of chlorotriazine reactive azo dyes with H2O2/UV', *Dyes and Pigments*, vol. 33, no. 4. pp. 281–298, 1997.

[5] B. J. Brüschweiler and C. Merlot, 'Azo dyes in clothing textiles can be cleaved into a series of mutagenic aromatic amines which are not regulated yet', *Regul. Toxicol. Pharmacol.*, vol. 88, pp. 214–226, 2017.

[6] R. Sasikala, K. Karthikeyan, D. Easwaramoorthy, I. M. Bilal, and S. K. Rani, 'Photocatalytic degradation of trypan blue and methyl orange azo dyes by cerium loaded CuO nanoparticles', *Environ. Nanotechnology, Monit. Manag.*, vol. 6, pp. 45–53, 2016.

[7] M. A. Abdullahi *et al.*, 'Photocatalytic Degradation of Azo Dyes and Organic Contaminants in Wastewater Using Magnetically Recyclable Fe3O4@UA-Cu Nano-catalyst', *Catal. Letters*, vol. 148, no. 4, pp. 1130–1141, Apr. 2018.

[8] The Royal Society of Chemistry, 'Etching time / min', *R. Soc. Chem.*, pp. 2–3, 2015.

[9] M. Beija, C. A. M. Afonso, and J. G. Martinho, 'Synthesis and applications of Rhodamine derivatives as fluorescent probes'.

[10] A. Hasanbeigi and L. Price, 'A technical review of emerging technologies for energy and water ef fi ciency and pollution reduction in the textile industry', *J. Clean. Prod.*, vol. 95, pp. 30–44, 2015.

[11] L. Zimmer, 'Chinese Textile Polluters Disregard Environmental Regulations, Says Report', *Ecouterre*, 2012.

[12] Z. Carmen and S. Daniel, 'Textile Organic Dyes – Characteristics, Polluting Effects and Separation/Elimination Procedures from Industrial Effluents – A Critical Overview', *Org. Pollut. Ten Years After Stock. Conv. - Environ. Anal. Updat.*, 2012.

[13] S. Sonia, S. Poongodi, P. S. Kumar, D. Mangalaraj, N. Ponpandian, and C. Viswanathan, 'Hydrothermal synthesis of highly stable CuO nanostructures for efficient photocatalytic degradation of organic dyes', *Mater. Sci. Semicond. Process.*, 2015.

[14] J.-M. Herrmann, 'Heterogeneous photocatalysis: fundamentals and applications to the removal of various types of aqueous pollutants', *Catal. Today*, vol. 53, pp. 115–129, 1999.

[15] J. Zhu, H. Bi, Y. Wang, X. Wang, X. Yang, and L. Lu, 'CuO nanocrystals with controllable shapes grown from solution without any surfactants', *Mater. Chem. Phys.*, vol. 109, no. 1, pp. 34–38, 2008.

[16] CSIR Ghana, 'Pollution of Ghana's water bodies ... CSIR predicts water crisis in 2030', *Csir Latest News*, 2017. [Online]. Available: http://www.csir.org.gh/index.php/component/k2/item/414-pollution-of-ghana-s-water-bodies-csir-predicts-water-crisis-in-2030?tmpl=component&print=1. [Accessed: 29-Sep-2017].

[17] CSIR South Africa, 'SA Climate experts warn of a drier future in Western Cape', *CSIR*,

2017. [Online]. Available: https://www.csir.co.za/sa-climate-experts-warn-drier-future-western-cape-0. [Accessed: 30-Sep-2017].

[18] R. Davies, 'Drought predictions for Southern Africa', *Mail & Guardian*, Sep-2015.

[19] United Nations, 'Goal 6 Clean Water and Sanitation.pdf', *Sustainable Development Goals*, 2015. [Online]. Available: http://www.gh.undp.org/content/ghana/en/home/post-2015/sdg-overview/goal-6.html. [Accessed: 29-Sep-2017].

[20] United Nations, 'Clean water and sanitation: Why it matters', *Sustainable Development Goals*, 2015. [Online]. Available: http://www.un.org/sustainabledevelopment/water-and-sanitation/. [Accessed: 29-Sep-2017].

[21] Green Earth Nanoscience Inc., 'What is Photocatalysis?', *Green Earth Nanoscience Inc.*, 2017. [Online]. Available: http://www.greenearthnanoscience.com/what-is-photocatalyst.php. [Accessed: 02-Oct-2017].

[22] K. Kabra, R. Chaudhary, and R. L. Sawhney, 'Treatment of Hazardous Organic and Inorganic Compounds through Aqueous-Phase Photocatalysis: A Review', *Ind. Eng. Chem. Res.*, vol. 43, no. 24, pp. 7683–7696, Nov. 2004.

[23] D. Robert and S. Malato, 'Solar photocatalysis: A clean process for water detoxification', *Sci. Total Environ.*, vol. 291, no. 1–3, pp. 85–97, 2002.

[24] R. P. Souza *et al.*, 'Photocatalytic activity of TiO2, ZnO and Nb2O5 applied to degradation of textile wastewater', *J. Photochem. Photobiol. A Chem.*, vol. 329, pp. 9–17, 2016.

[25] F. Peng, L. Cai, H. Yu, H. Wang, and J. Yang, 'Synthesis and characterization of substitutional and interstitial nitrogen-doped titanium dioxides with visible light

photocatalytic activity', *J. Solid State Chem.*, vol. 181, no. 1, pp. 130–136, 2008.

[26] J. Ma, K. Wang, L. Li, T. Zhang, Y. Kong, and S. Komarneni, 'Visible-light photocatalytic decolorization of Orange II on Cu2O/ZnO nanocomposites', *Ceram. Int.*, vol. 41, no. 2, pp. 2050–2056, Mar. 2015.

[27] G. Mustafa, M. I. Zafar, and M. A. Nadeem, 'Journal of Environmental Chemical Engineering Photocatalytic degradation of textile dyes on Cu2O-CuO/TiO2 anatase powders', vol. 4, pp. 2138–2146, 2016.

[28] T. H. Tran and V. T. Nguyen, 'Copper Oxide Nanomaterials Prepared by Solution Methods, Some Properties, and Potential Applications: A Brief Review', *Int. Sch. Res. Not.*, vol. 2014, pp. 1–14, 2014.

[29] W. Wang, L. Wang, H. Shi, and Y. Liang, 'A room temperature chemical route for large scale synthesis of sub-15 nm ultralong CuO nanowires with strong size effect and enhanced photocatalytic activity', *CrystEngComm*, 2012.

[30] L. J. Wang *et al.*, 'Size effect and enhanced photocatalytic activity of CuO sheet-like nanostructures prepared by a room temperature solution phase chemical method', *Appl. Surf. Sci.*, vol. 271, pp. 136–140, Apr. 2013.

[31] K. Zhou, R. Wang, B. Xu, and Y. Li, 'Synthesis, characterization and catalytic properties of CuO nanocrystals with various shapes', *Nanotechnology*, vol. 17, no. 15, pp. 3939–3943, 2006.

[32] A. Bello, D. Dodoo-Arhin, K. Makgopa, M. Fabiane, and N. Manyala, 'Surfactant Assisted Synthesis of Copper Oxide (CuO) Leaf-like Nanostructures for Electrochemical Applications', *Am. J. Mater. Sci.*, vol. 4, no. 2, pp. 64–73, 2014.

[33] Q. Zhang, K. Zhang, D. Xu, G. Yang, and H. Huang, 'Progress in Materials Science

CuO nanostructures : Synthesis , characterization , growth mechanisms , fundamental properties , and applications', *Prog. Mater. Sci.*, vol. 60, no. October 2013, pp. 208–337, 2014.

[34] O. K. Dalrymple, E. Stefanakos, M. A. Trotz, and D. Y. Goswami, 'A review of the mechanisms and modeling of photocatalytic disinfection', *Applied Catalysis B: Environmental*, vol. 98, no. 1–2. pp. 27–38, 2010.

[35] M. Vashistha, K. Kabra, V. Vyas, R. Kumar, B. K. Sharma, and G. Sharma, 'Electronic Structure of CuO from First-Principles and Experiment', *Quantum Matter*, vol. 5, no. 5, pp. 717–720, 2016.

[36] B. Himmetoglu, R. M. Wentzcovitch, and M. Cococcioni, 'First-principles study of electronic and structural properties of CuO', *Phys. Rev. B*, vol. 84, no. 11, p. 115108, Sep. 2011.

[37] L. Wang *et al.*, 'A facile room temperature solution-phase route to synthesize CuO nanowires with enhanced photocatalytic performance', *Mater. Lett.*, vol. 74, pp. 217–219, May 2012.

[38] Z. Yang, J. Xu, W. Zhang, A. Liu, and S. Tang, 'Controlled synthesis of CuO nanostructures by a simple solution route', *J. Solid State Chem.*, vol. 180, no. 4, pp. 1390–1396, 2007.

[39] A. Bhattacharjee and M. Ahmaruzzaman, 'CuO nanostructures: Facile synthesis and applications for enhanced photodegradation of organic compounds and reduction of: P -nitrophenol from aqueous phase', *RSC Adv.*, vol. 6, no. 47, pp. 41348–41363, 2016.

[40] D. Li *et al.*, 'CuO nanostructures prepared by a chemical method', *J. Cryst. Growth*, vol. 282, no. 1–2, pp. 105–111, 2005.

[41] M. Sahooli, S. Sabbaghi, and R. Saboori, 'Synthesis and characterization of mono sized CuO nanoparticles', *Mater. Lett.*, 2012.

[42] Q. Zhang, K. Zhang, D. Xu, G. Yang, and H. Huang, 'Progress in Materials Science CuO nanostructures : Synthesis , characterization , growth mechanisms , fundamental properties , and applications', *Prog. Mater. Sci.*, vol. 60, no. October 2013, pp. 208–337, 2014.

[43] A. Sadollahkhani, Z. Hussain, S. Elhag, O. Nur, and M. Willander, 'Photocatalytic properties of different morphologies of CuO for the degradation of Congo red organic dye', *Ceram. Int.*, vol. 40, no. 7, pp. 11311–11317, 2014.

[44] M. Rabbani, R. Rahimi, M. Bozorgpour, J. Shokraiyan, and S. S. Moghaddam, 'Photocatalytic application of hollow CuO microspheres with hierarchical dandelion-like structures synthesized by a simple template free approach', *Mater. Lett.*, vol. 119, pp. 39–42, 2014.

[45] L. J. Wang *et al.*, 'Size effect and enhanced photocatalytic activity of CuO sheet-like nanostructures prepared by a room temperature solution phase chemical method', *Appl. Surf. Sci.*, vol. 271, pp. 136–140, Apr. 2013.

[46] X. Liu, Z. Li, Q. Zhang, F. Li, and T. Kong, 'CuO nanowires prepared via a facile solution route and their photocatalytic property', *Mater. Lett.*, vol. 72, pp. 49–52, Apr. 2012.

[47] H. Ming *et al.*, 'Electrochemical fabrication of Cu(OH)2 and CuO nanostructures and their catalytic property', *J. Cryst. Growth*, 2011.

[48] A. P. Reverberi, N. T. Kuznetsov, V. P. Meshalkin, M. Salerno, and B. Fabiano, 'Systematical analysis of chemical methods in metal nanoparticles synthesis', *Theor.*

Found. Chem. Eng., vol. 50, no. 1, pp. 59–66, Jan. 2016.

[49] H. Siddiqui, M. S. Qureshi, and F. Z. Haque, 'Effect of copper precursor salts: Facile and sustainable synthesis of controlled shaped copper oxide nanoparticles', *Optik (Stuttg).*, vol. 127, no. 11, pp. 4726–4730, 2016.

[50] K. Bubacz, J. Choina, D. Dolat, and A. W. Morawski, 'Methylene blue and phenol photocatalytic degradation on nanoparticles of anatase TiO 2', *Polish J. Environ. Stud.*, vol. 19, no. 4, pp. 685–691, 2010.

[51] N. Riaz, F. K. Chong, B. K. Dutta, Z. B. Man, M. S. Khan, and E. Nurlaela, 'Photodegradation of Orange II under visible light using Cu–Ni/TiO2: Effect of calcination temperature', *Chem. Eng. J.*, vol. 185–186, pp. 108–119, Mar. 2012.

[52] National Center for Biotechnology Information, 'Methyl Orange', *PubChem Compound Database CID 23673835*, 2017. [Online]. Available: https://pubchem.ncbi.nlm.nih.gov/compound/23673835. [Accessed: 02-Oct-2017].

[53] C. Baiocchi, M. C. Brussino, E. Pramauro, A. B. Prevot, L. Palmisano, and G. Marci, 'Characterization of Methyl Orange and Its Photocatalytic Degradation Products by HPLC/UV-VIS Diode Array and Atmospheric Pressure Ionization Quadrupole Ion Trap Mass Spectrometry', *Int. J. Mass Spectrom.*, vol. 214, no. 2, pp. 247–256, 2002.

[54] M. Rosu *et al.*, 'Azo dyes degradation using TiO 2 -Pt / graphene oxide and TiO 2 -Pt / reduced graphene oxide photocatalysts under UV and natural sunlight irradiation', *Solid State Sci.*, vol. 70, pp. 13–20, 2017.

[55] A. Zaleska, 'Doped-TiO2: A Review', *Recent Patents Eng.*, vol. 2, no. 3, pp. 157–164, 2008.

[56] F. Peng, L. Cai, L. Huang, H. Yu, and H. Wang, 'Preparation of nitrogen-doped titanium

dioxide with visible-light photocatalytic activity using a facile hydrothermal method', *J. Phys. Chem. Solids*, vol. 69, no. 7, pp. 1657–1664, 2008.

[57] T. A. Saleh and V. K. Gupta, 'Photo-catalyzed degradation of hazardous dye methyl orange by use of a composite catalyst consisting of multi-walled carbon nanotubes and titanium dioxide', *J. Colloid Interface Sci.*, vol. 371, no. 1, pp. 101–106, 2012.

[58] N. Kislov, J. Lahiri, H. Verma, D. Y. Goswami, E. Stefanakos, and M. Batzill, 'Photocatalytic Degradation of Methyl Orange over Single Crystalline ZnO: Orientation Dependence of Photoactivity and Photostability of ZnO', *Langmuir*, vol. 25, no. 5, pp. 3310–3315, Mar. 2009.

[59] T. Chen, Y. Zheng, J.-M. Lin, and G. Chen, 'Study on the Photocatalytic Degradation of Methyl Orange in Water Using Ag/ZnO as Catalyst by Liquid Chromatography Electrospray Ionization Ion-Trap Mass Spectrometry', *J Am Soc Mass Spectrom*, vol. 19, pp. 997–1003, 2008.

[60] J. Fan, Y. Guo, J. Wang, and M. Fan, 'Rapid decolorization of azo dye methyl orange in aqueous solution by nanoscale zerovalent iron particles', *J. Hazard. Mater.*, vol. 166, no. 2–3, pp. 904–910, Jul. 2009.

[61] J. M. Peralta-Hernandez, Y. Meas-Vong, F. J. Rodriguez, T. W. Chapman, M. I. Maldonado, and L. A. Godinez, 'Comparison of hydrogen peroxide-based processes for treating dye-containing wastewater: Decolorization and destruction of Orange II azo dye in dilute solution', *Dye. Pigment.*, vol. 76, no. 3, pp. 656–662, 2008.

[62] K. Meerbergen *et al.*, 'Decolorization of reactive azo dyes using a sequential chemical and activated sludge treatment', *J. Biosci. Bioeng.*, vol. xx, no. xx, pp. 1–6, 2017.

[63] K. A. Tan, N. Morad, and J. Q. Ooi, 'Phytoremediation of Methylene Blue and Methyl

Orange Using Eichhornia crassipes', *Int. J. Environ. Sci. Dev.*, vol. 7, no. 10, pp. 724–728, 2016.

[64] G. K. Parshetti, A. A. Telke, D. C. Kalyani, and S. P. Govindwar, 'Decolorization and detoxification of sulfonated azo dye methyl orange by Kocuria rosea MTCC 1532', *J. Hazard. Mater.*, vol. 176, no. 1–3, pp. 503–509, Apr. 2010.

[65] L. Hua, H. Ma, and L. Zhang, 'Degradation process analysis of the azo dyes by catalytic wet air oxidation with catalyst CuO/gamma-Al2O3', *Chemosphere*, vol. 90, no. 2. pp. 143–149, 2013.

[66] V. Žunič, 'Photocatalytic discoloration of the azo dye methylene blue in the presence of irradiated TiO2/Pt nano-composite'.

[67] American Chemistry Council, 'Methylene Blue, Part 1: The Biologist's Dye', 2006. [Online]. Available: https://chlorine.americanchemistry.com/Science-Center/Chlorine-Compound-of-the-Month-Library/Methylene-Blue-Part-1-The-Biologists-Dye/. [Accessed: 05-Apr-2018].

[68] National Center for Biotechnology Information, 'Methylene Blue Anhydrous', *PubChem Compound Database; CID=6099*, 2018. [Online]. Available: https://pubchem.ncbi.nlm.nih.gov/compound/methylene_blue#section=Top. [Accessed: 05-Apr-2018].

[69] P. J. Rameshwar Ameta, Dileep Kumar, 'Photocatalytic degradation of methylene blue using calcium oxide', *Acta Chim. Pharm. Indica*, vol. 4, no. 1, pp. 20–28, 2014.

[70] A. Houas, H. Lachheb, M. Ksibi, E. Elaloui, C. Guillard, and J.-M. Herrmann, 'Photocatalytic degradation pathway of methylene blue in water', *Appl. Catal. B Environ.*, vol. 31, no. 2, pp. 145–157, May 2001.

[71] J. Rameshwar, A., Dileep, K., Priyanka, 'Photo catalytic Degradation Of Methylene Blue Using Calcium Oxide', *Acta Chim Pharm Indica*, vol. 4, no. 1, pp. 20–28, 2014.

[72] A. K. Menon and S. J. Kalita, 'Efficient Photocatalytic Degradation of Methylene Blue with CuO Loaded Nanocrystalline TiO2', Wiley-Blackwell, pp. 77–87.

[73] National Center for Biotechnology Information, 'Rhodamine B', *PubChem Compound Database; CID=6694*, 2018. [Online]. Available: https://pubchem.ncbi.nlm.nih.gov/compound/6694. [Accessed: 05-Apr-2018].

[74] S. Zaman, A. Zainelabdin, G. Amin, O. Nur, and M. Willander, 'Efficient catalytic effect of CuO nanostructures on the degradation of organic dyes', *J. Phys. Chem. Solids*, vol. 73, no. 11, pp. 1320–1325, Nov. 2012.

[75] H. Li, J. Liao, and T. Zeng, 'A facile synthesis of CuO nanowires and nanorods, and their catalytic activity in the oxidative degradation of Rhodamine B with hydrogen peroxide', *Catal. Commun.*, vol. 46, pp. 169–173, 2014.

[76] M. P. Rao, P. Sathishkumar, R. V. Mangalaraja, A. M. Asiri, P. Sivashanmugam, and S. Anandan, 'Simple and low-cost synthesis of CuO nanosheets for visible-light-driven photocatalytic degradation of textile dyes', *J. Environ. Chem. Eng.*, vol. 6, no. 2, pp. 2003–2010, 2018.

[77] A. Tadjarodi, O. Akhavan, and K. Bijanzad, 'Photocatalytic activity of CuO nanoparticles incorporated in mesoporous structure prepared from bis(2-aminonicotinato) copper(II) microflakes', *Trans. Nonferrous Met. Soc. China*, vol. 25, no. 11, pp. 3634–3642, Nov. 2015.

[78] Y. Cudennec and A. Lecerf, 'The transformation of Cu(OH)2 into CuO, revisited', *Solid State Sci.*, vol. 5, no. 11–12, pp. 1471–1474, Nov. 2003.

[79] P. K. Raul *et al.*, 'CuO nanorods: A potential and efficient adsorbent in water purification', *RSC Adv.*, vol. 4, no. 76, pp. 40580–40587, 2014.

[80] G. Kliche and Z. V Popovic, 'Far-infrared spectroscopic investigations on CuO', *Phys. Rev. B*, vol. 42, no. 16, pp. 10060–10066, 1990.

[81] A. S. Ethiraj and D. J. Kang, 'Synthesis and characterization of CuO nanowires by a simple wet chemical method.', *Nanoscale Res. Lett.*, vol. 7, no. 1, p. 70, Jan. 2012.

[82] K. K. Dey *et al.*, 'Growth morphologies, phase formation, optical & biological responses of nanostructures of CuO and their application as cooling fluid in high energy density devices', *RSC Adv.*, vol. 2, no. 4, pp. 1387–1403, 2012.

[83] M. D. Donohue and G. L. Aranovich, 'Classification of Gibbs adsorption isotherms', *Adv. Colloid Interface Sci.*, vol. 76–77, no. October, pp. 137–152, 1998.

[84] D. Dollimore, P. Spooner, and A. Turner, 'The BET method of analysis of gas adsoprtion and its relevance to the calculation of surface area', *Surf. Technol.*, vol. 4, pp. 121–160, 1976.

[85] D. P. Dubal, G. S. Gund, C. D. Lokhande, and R. Holze, 'CuO cauliflowers for supercapacitor application: Novel potentiodynamic deposition', *Materials Research Bulletin*, vol. 48, no. 2. pp. 923–928, 2013.

[86] S. E. Kentish, C. A. Scholes, and G. W. Stevens, 'Carbon Dioxide Separation through Polymeric Membrane Systems for Flue Gas Applications', *Recent Patents Chem. Eng.*, vol. 1, no. 1, pp. 52–66, Jan. 2010.